SorCS2 binds progranulin and regulates motor axon outgrowth

Thomasen PB[1,2], Salašová A[1,2], Login H[1,2], Beel S[3], Tranberg-Jensen J[1,2], Qvist P[2], Ovesen PL[1,2], Nolte S[1,2], Nejsum LN[4], Chao MV[5], Dasen J[5], Van Damme P[3], Kjaer-Sorensen K[6], Oxvig C[6], Nykjaer A[1,2,7].

1. Danish Research Institute of Translational Neuroscience DANDRITE-Nordic EMBL Partnership for Molecular Medicine, and Center of Excellence PROMEMO, Aarhus C, Denmark.
2. Department of Biomedicine, Aarhus University, Aarhus C, Denmark.
3. Department of Neurology and Department of Neurosciences, KU Leuven, Belgium and Center for Brain & Disease Research VIB, Leuven, Belgium.
4. Department of Clinical Medicine, Aarhus University, Aarhus N, Denmark.
5. Department of Neuroscience and Physiology, NYU Langone Health, New York, US.
6. Department of Molecular Biology and Genetics, Aarhus University, Aarhus C, Denmark.
7. Department of Neurosurgery, Aarhus University Hospital, Denmark.

Correspondence:

Anders Nykjaer
Department of Biomedicine
Høegh-Guldbergsgade 10, Bldg. 1115-1116
Aarhus University
DK-8000 Aarhus C
Denmark

Email: an@biomed.au.dk
Phone: +45 2899 2384

Abstract

Motor neuron development requires an orchestrated action of trophic factors and guidance cues for axons to reach their targets. Here, we identify SorCS2 as a novel receptor for progranulin (PGRN) that is required for motor axon outgrowth in zebrafish and mice. In both species motor neurons express SorCS2, and PGRN is produced in cells juxta-positioned the projecting axon, but in mice the neurons also co-express PGRN. In zebrafish, *sorcs2* knockdown produces stunted and aberrantly branched motor axons, and in *Sorcs2*$^{-/-}$ mice, forelimb innervation and motor neuron regeneration are substantially perturbed; phenotypes also observed in fish and mice lacking PGRN. SorCS2 binds PGRN and while motor neuron cultures from wildtype mice respond to exogenous PGRN by axon outgrowth, knockout neurons are unresponsive. Remarkably, when co-expressed in the same cells, SorCS2 controls secretion of PGRN. We conclude that SorCS2 navigates motor neuron development and enables axon regeneration through binding of PGRN.

Introduction

Motor neurons are the final relay that transmits signals from the central nervous system to skeletal muscles in the periphery, thereby enabling muscle contraction and movement. Their development is complex and requires a concerted action of trophic factors and guidance cues that secures neuronal survival, axonal outgrowth and the proper formation of functional neuromuscular junctions (NMJs). This process relies on signaling molecules expressed by the motor neurons themselves as well the surrounding cells in a manner that is highly controlled in time and space[1,2]. The same neurotrophic factors and guidance cues are often reactivated during axonal regeneration after peripheral nerve injury, as they support neuronal survival and navigate the axonal regrowth following Wallerian degeneration[3]. Though motor axon outgrowth has been extensively studied in both mice and zebrafish, the proteins and pathways involved are still not fully understood.

The Vps10p-domain (Vps10p-d) receptor, SorCS2, is a member of the sortilin receptor family comprising sortilin, SorLA, SorCS1, and SorCS3. The receptors predominate in distinct neuronal populations of the central- and peripheral nervous system where they bind a vast number of ligands and engage in cell signaling, endocytosis, and intracellular trafficking[4,5]. The expression of SorCS1, -2, and -3 dynamically changes during embryonic development, suggesting important roles in defining neuronal structures[6–11]. Conceptually, signaling through a Vps10p-d receptor requires formation of heteromeric complexes with the ligand and a co-receptor[5,12,13]. By doing so, SorCS2 has been implicated in activities ranging from growth cone retraction, to regulation of neuronal plasticity and apoptosis of peripheral glia[13–17].

All Vps10p-d receptors are initially produced as a proform containing a propeptide that is cleaved off in the late Trans-Golgi Network (TGN) to generate a mature single-chain receptor. However, SorCS2 stands out from the other family members as it can be further converted from the single-chain form that controls growth cone retraction and synaptic plasticity, into a two-chain variant that is proapoptotic when expressed in glia cells[13,16]. The sorting activities of the receptor family are many and each receptor may engage in several trafficking pathways to control ligand secretion, endocytosis, recycling, and lysosomal sorting from the TGN. Notably, SorCS2 can establish the surface exposure and synaptic targeting of membrane receptors such as the tyrosine receptor kinase, TrkB, and NMDA receptors[16–18].

PGRN is a multifunctional protein produced by several cell types including microglia and neurons[19]. Among other functions, it promotes neuronal development and repair, sustains neuronal integrity,

and suppresses neuroinflammatory responses[20–22]. For instance, motor neuron development is substantially perturbed in zebrafish lacking PGRN and in *Grn* knockout mice regeneration of injured motor neurons is delayed[23–27]. The neuroprotective effect of PGRN is further supported by *GRN* haploinsufficiency being a common cause of frontotemporal dementia[19,28,29]. Molecularly, PGRN exerts its pleiotropic functions by two mechanisms. It can signal cross the plasma membrane, and it can sustain lysosomal function by providing mature granulins and by targeting the enzyme prosaposin to lysosomes[20,21,27,30]. Whereas the pathways that mediate lysosomal sorting have been extensively studied[31–33], the receptor(s) responsible for binding PGRN and transducing its neurotrophic activity remains elusive.

Here we show that SorCS2 regulates motor neuron outgrowth in fish and mice. In both species, SorCS2 inactivation resulted in stunted motor neurons, and in SorCS2 knockout (*Sorcs2*$^{-/-}$) mice regeneration of injured adult motor neurons was perturbed too. Further, we demonstrate that SorCS2 binds PGRN to facilitate its cellular signaling and secretion. Our findings identify SorCS2 as a novel PGRN receptor and highlight the importance of this interaction for motor neuron development and regeneration.

Results

Sorcs2 is expressed in motor neurons in the ventral spinal cord of zebrafish embryos

To interrogate the function of SorCS2 in motor neuron development we first assessed its embryonic expression in zebrafish. *sorcs2* was weakly expressed in embryos from 12 hours post fertilization (hpf) and increased during development up to 48 hpf (**Fig. 1A**). We subsequently analysed its tissue expression by alkaline *in situ* hybridisation (ISH) at 24 hpf, a time point when many mechanisms regulating motor neuron development are active (**Fig. 1B)**. *sorcs2* was detected in the ventral spinal cord corresponding to the location of motor neurons as well as in muscle cells within the somites (**Fig. 1B**). To enhance resolution of the ISH we employed third generation *in situ* hybridization chain reaction (*in situ* HCR v3.0)[34] on transgenic fish expressing GFP driven by the motor neuron-specific promotor *mnx1 (Tg(mnx1:GFP)*^{ml2}*)*. In accordance with the regular ISH, we detected *sorcs2* mRNA in motor neuron cell bodies in the spinal cord and in muscle in the trunk at 24 hpf as shown by lateral view (**Fig. 1C-D**) and in cross sections (**Fig. 1E-F**). Analysis for *sorcs2* expression using a single-cell transcriptome atlas of zebrafish embryos[35] (**Fig. S1A-C**) confirmed our *in situ* HCR data.

106 ***Sorcs2* knockdown causes stunted and aberrantly branched motor axons**

107 To study the impact of SorCS2 deficiency on motor neuron outgrowth, we knocked down (KD)
108 receptor expression by injecting a morpholino oligomer that disrupts a splice site in *sorcs2* (sMO).
109 At a dosage of 3.7 ng, the sMO effectively perturbed *sorcs2* splicing at 24 hpf **(Fig. 1G)** with no
110 effect on developmental rate or morphology (**Fig. S2**). We assessed motor neuron length and
111 branching in sMO-injected embryos at 27 hpf by whole-mount immunofluorescence (IF) staining
112 using a znp-1 antibody that labels Synaptotagmin 2 (**Fig. 1H)**. Zebrafish have three primary motor
113 neurons innervating each somatic hemisegment, where the axon of the caudal primary motor neuron
114 (CaP) is the first to grow, extending its projection into the ventral somite as indicated in **Fig. 1I-J**. In
115 control-injected embryos, 95.6% of the CaP axons reached the distal ventral myotome (DVM), and
116 all axons extended beyond the notochord (**Fig. L**). In contrast, axons of *sorcs2* KD embryos were
117 stunted with 81.9% of axons reaching the DVM and 1.9% only reaching the horizontal myoseptum
118 (HMS) ($p < 0.0001$). In addition, 16.5% of the axons were branched in *sorcs2* KD larvae compared
119 to 5.9% in control ($p < 0.0001$), and severe branching was only observed in the sMO-injected group
120 (**Fig. 1M**). Confirming the causative effect of *sorcs2* knockdown on these phenotypes, co-injection
121 with the human *SORCS2* mRNA fully rescued the phenotype to the extent that 97.5% of the axons
122 now exhibited normal growth ($p < 0.0001$) and 7% displayed branching ($p < 0.0001$) (**Fig. 1L-M**).
123 We further analysed motor neuron length in *sorcs2* knockout embryos (*sorcs2*$^{-/-}$) from heterozygous
124 cross of the *sorcs2*^{sa11642} fish line that harbors a disruptive mutation in exon 10. Similar to KD larvae,
125 *sorcs2*$^{-/-}$ embryos exhibited stunted CaP axons as only 83.4% of axons reached the DVM compared
126 to 97% in wildtype (wt) siblings ($p = 0.022$) (**Fig. S3A**). Injection of the sMO into the *sorcs2*$^{-/-}$
127 embryos did not further aggravate the motor neuron phenotype (**Fig. S3B**), which validates that the
128 sMO is specific and has no off-target effects. Because of poor breeding of the *sorcs2*^{sa11642} fish, we
129 continued our studies using the KD model.

130 To determine the dynamics of the outgrowth of the CaP axons in *sorcs2* deficient embryos, we
131 subjected *Tg(mnx1:GFP)*^{ml2} zebrafish to time-lapse imaging. CaP axons exit the spinal cord around
132 16-18 hpf and reach the HMS around 20-24 hpf where they make the first synaptic contacts. They
133 pause here for a few hours before continuing ventrally into the myotome[36]. In *sorcs2* KD embryos
134 axons paused for a longer period at the HMS though they retained their ability to extend beyond the
135 choice point and grow ventrally (**Fig. 2A, Suppl. Movie 1-2**). However, several axons remained
136 truncated and some started branching prematurely at later stages.

137

138 **Perturbed acetylcholine receptor clustering and motility in *sorcs2* KD embryos**

139 Given the aberrant motor axon outgrowth in *sorcs2* deficient embryos, we asked whether axons
140 were still capable of forming functional synapses with the acetylcholine receptors (AChRs) at the
141 NMJ. To address this, co-staining of the motor axons and AChR clusters was performed at 27 and
142 48 hpf. During normal development, a prepattern of AChR clusters are partly replaced by
143 neuromuscular synapses at 27 hpf. AChRs are clustered beneath outgrowing motor axons but are
144 not yet precisely colocalized with clusters of synaptic vesicles in nascent presynaptic terminals.
145 Further, diffuse non-clustered AChRs are present at the yet non-innervated myoseptum, which
146 separates adjacent myotomes[37]. This pattern we observed in control-injected embryos in which
147 motor axons co-localized with AChR clusters (**Fig. 2B**). In marked contrast, AChR clusters in the
148 *sorcs2* KD embryos were elongated and diffuse thereby resembling the pattern of immature, non-
149 innervated clusters present at earlier stages of development. Similarly, co-localization between
150 axons and AChRs were incomplete (arrows, **Fig. 2B**). Co-injection with human *SORCS2* mRNA
151 fully rescued the phenotype. At 48 hpf motor axons have normally extended their branches into
152 laterally located muscle fibres and turned at the edge of the myotome into the myosepta[37]. We
153 found that in *sorcs2* KD embryos, axons had advanced less into the myosepta both in the ventral
154 and dorsal direction. Furthermore, the co-localization between axon branches and AChRs in the
155 somites remained reduced (asterisks, **Fig. 2B**). At this stage, *in situ* HCR on *Tg(mnx1:GFP)^{ml2}*
156 embryos showed that *sorcs2* was still highly expressed in motor neurons (**Fig. 2C-D**).

157 Prompted by the impaired synapse development, we next assessed the embryonic motility. We used
158 a touch response assay[38] in which the motility of 48 hpf embryos is assayed as the time it takes to
159 swim 1 cm after a light touch. Here, the *sorcs2* KD embryos showed a significantly slower escape
160 response and they spent on average 183 ms to swim 1 cm compared to the control embryos that
161 only used 98 ms (**Fig. 2E-F**, $p = 0.008$, **Suppl. Movie 3-4**). Taken together our results demonstrated
162 that SorCS2 is required for proper motor neuron development, NMJ maturation, and motor function
163 in zebrafish.

164 **Impaired motor axon outgrowth in *Sorcs2$^{-/-}$* mice**

165 Given the phenotype in zebrafish and that SorCS2 is highly conserved among species, we
166 speculated that SorCS2 might also be critical for motor neuron development in mice. Murine, spinal
167 motor neurons develop from progenitor cells located in the medial neural tube. They progress into
168 postmitotic neurons around E9.5 and migrate laterally to position themselves into specific motor
169 columns according to the muscle fibres they innervate[1,39]. Motor axons exit the spinal cord mainly

170 through the ventral roots and innervate their target muscle around E13-E14[1,40]. Accordingly, we
171 first determined the expression pattern of SorCS2 in E12.5 mouse embryos by IF staining (**Fig. 3A-**
172 **C**). At the brachial level, SorCS2 was highly expressed in the floor plate and the ventral spinal cord
173 where motor neurons are located, whereas staining was absent in the dorsal spinal cord and dorsal
174 root ganglion that contain sensory neurons. At this age SorCS2 was also present in skeletal muscle,
175 oesophagus, trachea, and boundary cap cells lining the entry and exit points of the peripheral nerve
176 roots (**Fig. 3A**). Co-staining for Hb9 and Foxp1, markers that specify most of the spinal motor
177 neurons and designate the limb-innervating lateral column of motor neurons at brachial and lumbar
178 levels[1,41], respectively, showed prominent co-expression with SorCS2 (**Fig. 3A-C**).

179 Given the expression of SorCS2 in Hb9- and Foxp1-postive motor neurons, we asked whether *Sorcs2*$^{-}$
180 $^{/-}$ mice, like the zebrafish, display innervation deficits. Hence, knockout mice were crossed with
181 *Hb9::GFP* transgenic mice, and innervation of the forelimbs and trunk was visualized by whole-
182 mount imaging for GFP (**Fig. 3D-E)**. Notably, in the absence of SorCS2, axonal outgrowth was
183 substantially compromised. The ulnar nerve was 18% shorter in the SorCS2-deficient animals (**Fig.**
184 **3F**, wt: 774 µm, *Sorcs2*$^{-/-}$: 630 µm, p = 0.0048), and the medial anterior thoracic nerve that innervates
185 the cutaneous maximus and anterior latissimus dorsi muscles was 31% shorter compared to wt mice
186 (wt: 783 µm, *Sorcs2*$^{-/-}$: 539 µm, p = 0.0048). Further, the total area covered by the terminal axon
187 arbors of the medial anterior thoracic nerve was reduced by no less than 52% (wt: 153,763 µm^2,
188 *Sorcs2*$^{-/-}$: 73,984 µm^2, p = 0.0034) (**Fig. 3G**). In contrast, SorCS2 expression did not impact the
189 thickness of the motor nerves (**Fig. 3H**). We conclude that SorCS2 is required for proper motor
190 neuron development also in mice.

191 **Binding of progranulin to SorCS2 and their expression in zebrafish and mice**

192 We tested a panel of proteins implicated in axon pathfinding and trophic support for binding to
193 SorCS2 using surface plasmon resonance (SPR) analysis and cellular binding assays. We failed to
194 detect any consistent binding of EphrinA1-5, EphrinB1-3, EphA1-8, EphB1-6, UNC5H4, and
195 netrin-1 in either of the assays (data not shown). However, PGRN bound robustly to the
196 extracellular domain of SorCS2 by SPR analysis with an affinity of ~3 nM (**Fig. 4A**). This was
197 intriguing since knockdown of the PGRN-A encoding gene (*grna*) in zebrafish phenocopies the
198 truncation defects and premature branching of motor neurons present in the *sorcs2* KD embryos[23–
199 25]. Hence, we speculated that SorCS2 could be required to control PGRN function. To test this
200 hypothesis, we first probed PGRN expression during motor neuron development in zebrafish and

201 mice. Though the expression was generally sparse, *in situ* HCR revealed *grna* mRNA in zebrafish
202 embryos in cells along the yolk extension most likely corresponding to immune cells (arrow heads,
203 **Fig. 4B-C**). Strikingly, mRNA transcripts were also present in cells located in close proximity to
204 the motor neurons (arrows, **Fig. 4B-C**). At 24 hpf, *grna* transcripts were most abundant
205 juxtapositioned the initial segment of the projecting motor axons (**Fig. 4B**), whereas at 27 hpf *grna*
206 was now located more distally lining the motor axons in both the ventral and dorsal myotome (**Fig.**
207 **4C-E**). Analysis of deposited single-cell transcriptome data[35] suggested that the *grna* expressing
208 cells were accounted for by macrophages and neutrophils. In accordance with our *in situ* HCR data,
209 *Grna* was not detectable in motor neurons (**Fig. S4A-C**).

210 We next studied PGRN expression in sections of the spinal cord from E12.5 *Hb9::GFP* mice by IF
211 microscopy (**Fig. 4F-H**). We found that PGRN, like SorCS2 (cf. **Fig. 3A-C**), was present in Hb9-
212 postive neurons (arrow heads, **Fig. 4G**). RNA scope ISH confirmed this expression pattern and
213 further demonstrated that *Sorcs2* transcripts are abundant in the motor neurons too (**Fig. S5**).
214 Interestingly, some cells scattered throughout the embryo showed particularly bright PGRN
215 labelling. IF microscopy revealed these cells to co-express Iba-1, which designates microglia and
216 macrophages (**Fig. 4F-H**). Strikingly, outside the spinal cord PGRN expression was enriched in
217 Iba-1-positive macrophages flanking the projecting motor axon (arrows, **Fig. 4H**). Taken together
218 the data suggests that progranulin inside the motor neurons or secreted by cells surrounding the
219 growing axon may enable motor development through binding to SorCS2.
220

221 **PGRN-induced motor neurite outgrowth requires SorCS2 expression**

222 We next compared neurite outgrowth and sprouting in primary motor neurons isolated from E13.5[42]
223 wt and *Sorcs2*$^{-/-}$ mice cultured for four days in the absence or presence of exogenous PGRN (1.5
224 nM) or BDNF (0.4 nM) as a positive control. Labelling for β-tubulin was used to visualize neurites
225 and quantify their length and branching (**Fig. 5A**). Whereas we did not observe any effect on the
226 number of branches in wt neurons following PGRN stimulation (**Fig. 5B**), total neurite length was
227 increased by 46% from 156 μm to 227 μm ($p = 0.0001$) (**Fig. 5C**). The failure to stimulate
228 branching likely reflects that higher PGRN concentrations are required to induce sprouting of motor
229 neurons as previously published[43]. In marked contrast to wt mice, *Sorcs2*$^{-/-}$ motor neurons were
230 completely refractory to PGRN, as the total neurite length was identical to that of the unstimulated
231 cultures (no stimulation: 156 μm, PGRN: 157 μm) (**Fig. 5E**). This was not accounted for by an
232 intrinsic failure of the neurons to respond to trophic stimulation, since addition of BDNF increased

233 both branching and neurite length in the *Sorcs2*$^{-/-}$ cultures (no stimulation: 2.14 branches, BDNF:
234 3.39 branches, $p < 0.0001$, and total length BDNF: 156 vs. 212 µm, $p = 0.0001$) (**Fig. 5D-E**). This
235 was also seen for MNs from wt mice (2.16 branches vs. 3.46, $p < 0.0001$, and 156 µm vs. 246 µm, p
236 < 0.0001) (**Fig. 5B-C)**. Comparisons of the total branching and neurite length between genotypes
237 showed that cultured motor neurons grew to a similar extent and responded equally well to BDNF
238 treatment (branching: $p = 0.997$, length: $p = 0.395$), whereas the PGRN-induced increase in neurite
239 length was significantly different between wt neurons compared to *Sorcs2*$^{-/-}$ ($p = 0.0099$) (**Fig. 5F-**
240 **G**). We conclude that SorCS2 is required for PGRN-dependent motor neuron outgrowth *in vitro*.
241

242 **SorCS2 and PGRN are co-expressed in motor neurons postnatally**

243 During postnatal development, the dendritic tree of the motor neurons grows to attain their maturity
244 and to establish fully functioning synapses[44]. In the adult mouse PGRN supports neuronal function
245 and is neuroprotective[33,45]. Hence, we explored SorCS2 and PGRN expression in motor neurons of
246 the ventral horn in P3 (postnatal day 3) and adult mice 12 weeks of age. Double immunostaining for
247 GFP and the motor neuron marker choline acetyltransferase (ChAT) in *Hb9::GFP* mice confirmed
248 that Hb9 labels motor neurons also in the postnatal period (**Fig. 6A**). We found that SorCS2 and
249 PGRN were abundant in *Hb9::GFP*-positive neurons, where they predominated in perinuclear
250 vesicles in a pattern resembling that of the TGN (arrow heads, **Fig. 6B-C**). Furthermore, we extracted
251 RNA sequencing data from laser-captured micro-dissected motor neurons[46] to evaluate
252 transcriptional profiles of *Sorcs2* and *Grn* in the spinal cord, the facial nucleus, and the cranial nuclei
253 3 and 4 in P2, P5, and P10 mice. The data showed that *Grn* and *Sorcs2* expression is not restricted to
254 motor neurons originating from the spinal cord during the early postnatal period (**Fig. 6D**). In 12-
255 weeks-old mice, RT-qPCR demonstrated that *Sorcs2* mRNA transcripts are prominent in the spinal
256 cord as it is expressed to a level comparable to that in cortex (**Fig. 6E**). Protein expression was
257 validated by immunoblotting (**Fig. 6F**), and IF microscopy of serial sections showed that in the spinal
258 cord SorCS2 protein was restricted to ChAT+ motor neurons (**Fig. 6G-I**). Similarly, we detected
259 PGRN in the adult spinal cord with expression being enriched in motor neurons (**Fig. S6A-C**); an
260 observation that has also been reported by others[21]. Taken together, the data demonstrate that during
261 early postnatal stages and in the adult mouse SorCS2 and PGRN are co-expressed in motor neurons
262 suggesting a possible interaction inside the cell or at the cell surface following autocrine secretion.
263

264 ***Sorcs2*$^{-/-}$ mice show delayed functional recovery after facial nerve crush injury**

265 PGRN was recently found to support axonal outgrowth in adult mice as *Grn*$^{-/-}$ mice showed delayed
266 recovery after a facial nerve injury[27]. The facial nerve is made up entirely by motor axons originating
267 from the facial motor nucleus in the brain stem that is required to move the whiskers (**Fig. 7A**).
268 Double immunostaining with SMI-32 showed that SorCS2 was present in these motor neurons that
269 previously have been reported also to express PGRN[27] (**Fig. 7B**). We therefore investigated
270 regeneration of the facial nerve in *Sorcs2*$^{-/-}$ mice following an injury by applying the paradigm used
271 in the study on *Grn*$^{-/-}$ mice[27]. In this paradigm, the facial nerve is gently crushed distal to the
272 retroauricular branch on one side, and the uninjured contralateral side is used as an internal control
273 (**Fig. 7C**). After the crush, injured axons are lost and the whiskers become immobile. Regeneration
274 is subsequently assessed by scoring provoked whisker movement twice a day. Whereas wt mice were
275 fully recovered within 12 days, 14 days were required for the *Sorcs2*$^{-/-}$ mice (**Fig. 7D**). Quantified as
276 the area under the curve of whisker movement, recovery was significantly delayed in the knockouts
277 ($p < 0.001$) (**Fig. 7E**). Remarkably, the delayed recovery in the SorCS2 knockouts fully phenocopied
278 that previously observed for *Grn*$^{-/-}$ mice[27]. Our data suggest that SorCS2 may control PGRN activity
279 when co-expressed in the adult motor neurons during regeneration.

280

281 **SorCS2 binds PGRN to control its secretion**

282 Given the direct binding of PRGN to SorCS2 and the requirement of SorCS2 for motor neurons to
283 respond to exogenous PGRN by axon outgrowth (cf. **Figs. 4A and 5G**), we co-cultured HEK293
284 cells transfected with either PGRN or SorCS2, reasoning that the secreted PGRN would bind to
285 neighbouring SorCS2-positive cells (*trans*-interaction). Surprisingly, we failed to detect any *trans*-
286 interaction whether analysed by double IF microscopy (**Fig. 8A**) or by co-immunoprecipitation (co-
287 IP) with anti-PGRN and probing the precipitate for SorCS2 (**Fig. 8C**). Similar results were obtained
288 with N-terminally HA-tagged PGRN, which excludes the possibility that anti-PGRN antibody would
289 occupy the binding site for SorCS2 (**Fig. S7A+C**). The result follows other studies demonstrating
290 that at the plasma membrane, SorCS2 requires a co-receptor to efficiently bind its extracellular
291 ligands[13].

292 Aside from signaling[13–15], SorCS2 also mediates endocytosis and intracellular trafficking[16,18,47]. To
293 assess whether SorCS2 and PGRN may bind in a *cis*-configuration, HEK293 cells were co-transfected
294 to express both proteins simultaneously. We found that SorCS2 and PGRN strongly co-localized in
295 a perinuclear compartment and to a lesser extent in vesicles dispersed throughout the cytoplasm,

296 likely representing TGN, endosome and recycling vesicles (**Fig. 8B, S7B**). To demonstrate a physical
297 interaction between the proteins in *cis*, PGRN was immunoprecipitated and the precipitate
298 immunoblotted for SorCS2 (**Fig. 8C**). Remarkably, we found that PGRN bound SorCS2 and that this
299 interaction was restricted to the proform of the receptor that is enriched in the TGN. A similar result
300 was found when overexpressing HA-PGRN (**Fig. S6C**). Notably, overexpression of SorCS2 resulted
301 in a ~300% increase in cell-associated PGRN ($p = 0.0076$) (**Fig. 8C+E, S7C**), that was paralleled by
302 a corresponding decrease in PGRN secretion ($p = 0.0010$) (**Fig. 8D+F, S7D**). The total amount of
303 PGRN produced by the cells, meaning the sum of PGRN in the medium and lysate, was decreased
304 too, suggesting that SorCS2 may control PGRN secretion and potentially also its trafficking from the
305 TGN to lysosomes for degradation or processing into granulins (**Fig. 8G**, $p = 0.0068$). To assess
306 whether SorCS2 also alters PGRN levels when expressed at endogenous levels, we measured its
307 expression in the spinal cord of *Sorcs2*$^{-/-}$ mice. In contrast to cells overexpressing SorCS2, PGRN in
308 the spinal cord at P3 was increased by 240% in *Sorcs2*$^{-/-}$ mice (**Fig. 8H-I**, $p = 0.0017$) despite identical
309 mRNA levels (**Fig. 8J**). An increase in PGRN was confirmed using another antibody and cohort of
310 animals (49% increase, $p = 0.015$) (**Fig. S7E**). Overall, we conclude that SorCS2 can bind and retain
311 PGRN in the biosynthetic pathway thereby regulating its secretion and extracellular concentration.
312

313 ## Discussion

314 In this study, we identified SorCS2 as a novel regulator of motor axon outgrowth. Knockdown of
315 *sorcs2* in zebrafish embryos resulted in delayed axon development and aberrant branching, defects in
316 NMJ synapse formation, and ultimately in reduced motility. In *Sorcs2*$^{-/-}$ mice, innervation of the
317 forelimbs and the upper trunk at E12.5 was substantially compromised as manifested by shorter axons
318 and a reduced area covered by the terminal motor axon arbors. The functional recovery after a facial
319 nerve injury was markedly slowed in the SorCS2-deficient mice too, which demonstrates a critical
320 function of the receptor also in motor neuron regeneration.

321 We and others previously showed that SorCS2 regulates axonal innervation in the central nervous
322 system, as binding of proBDNF or proNGF to SorCS2 in complex with p75^{NTR} causes growth cone
323 collapse of CNS neurons[13–15]. As a consequence, *Sorcs2*$^{-/-}$ mice exhibit dopaminergic
324 hyperinnervation of the prefrontal cortex[13]. Here we found that in motor neurons, SorCS2 enables
325 axon outgrowth rather than its retraction, suggesting SorCS2 may induce opposing effects in distinct
326 types of neurons. In support of neuron differentiated functions, primary motor neurons from the

327 *Sorcs2*$^{-/-}$ mice responded to BDNF by axonal outgrowth and branching, whereas hippocampal neuron
328 cultures have been shown not to do so[16].

329 From a panel of proteins implicated in motor neuron development, we found robust binding of PGRN
330 to SorCS2. The activities of PGRN are multiple and several receptors have been suggested. When
331 bound to TNF receptor I/II, Toll-like receptor 9 and EphA2, PGRN may elicit anti-inflammatory
332 effects and modulate innate immunity and angiogenesis, respectively[48–50]. The mechanisms
333 underlying the trophic responses are less well understood. Notably however, it has been demonstrated
334 that PGRN engagement of Notch receptors promote motor neuron survival and regeneration[51].
335 Sortilin, a paralogue of SorCS2 and the first PGRN receptor to be identified, efficiently binds and
336 mediates endocytosis and lysosomal sorting of PGRN[31] but the trophic effects of PGRN is
337 independent of this receptor[43,52]. These observations are in marked contrast to those for SorCS2, as
338 SorCS2 was required for PGRN to elicit its neurotrophic effects.

339 During development we found SorCS2 expression in motor neurons, whereas PGRN is abundant in
340 cells in close proximity to the projecting axons. In E12.5 mice, the PGRN expressing cells were
341 positive for Iba-1, corroborating previous reports that find PGRN is enriched in immune cells
342 including macrophages and microglia of embryonic zebrafish and mice[53,54]. PGRN is also secreted
343 by activated Schwann cells following sciatic nerve injury to promote regrowth of their neighboring
344 neurons[55]. Interestingly, zebrafish Schwann cells are derived from neural crest cells that migrate
345 along the motor axons[56] correlating well with our observed *grna* expression pattern. Similar to
346 microglia, neural crest cells can secrete factors to change their microenvironment[57] and they may
347 represent another source of PGRN. Taken together, the expression patterns suggest that PGRN
348 released by Iba-1+ and Schwann cells, potentially also neural crest cells, may induce its neurotrophic
349 effect on developing and regenerating motor neurons through binding to SorCS2.

350 Surprisingly, we failed to demonstrate *trans*-binding in transfected HEK293 cells, but various
351 possibilities may explain this apparent paradox between lack of binding and biological activity.
352 PGRN can be cleaved into individual granulins, GRN A-G, upon secretion[58]. The neurotrophic effect
353 of PGRN is reliant on GRN E, as GRN E alone can induce survival and neuronal outgrowth, whereas
354 PGRN without the GRN E domain lacks this capacity[20,52]. Previous studies demonstrated that GRN
355 E is responsible for PGRN binding to sortilin suggesting the same may also apply for SorCS2[31]. We
356 used antibodies directed against full-length PGRN and we cannot discount the possibility that GRN
357 E is detected less efficiently, or that binding to SorCS2 sterically hinders subsequent antibody

358 binding. This may also explain why we did not detect binding with the N-terminally HA-tagged
359 PGRN when probed with the anti-HA antibody. A more intriguing explanation, however, is the
360 requirement of a co-receptor for SorCS2. Conceptually, Vps10p-d receptors partner with co-receptors
361 to form composite high affinity ligand binding sites[5,59]. For instance, the affinity of proNGF to sortilin
362 is increased by 20-fold when in complex with $p75^{NTR}$ [12], and binding of proBDNF to SorCS2 or
363 $p75^{NTR}$ individually is barely detectable but when co-expressed surface labeling is greatly enhanced[13].
364 Likewise, it is possible that in addition to SorCS2, a co-receptor is required for PGRN to efficiently
365 bind to the cell surface. This co-receptor may be absent from the SorCS2-transfected HEK293 cells,
366 whereas in cultured motor neurons that respond to PGRN by neurite outgrowth, it is present. The
367 identity of said co-receptor remains to be established but given PGRN can bind Notch receptors to
368 stimulate nerve regeneration, it makes them good candidates[51].

369 At E12.5 and in adult mice, we found that PGRN is also expressed by motor neurons. In these neurons
370 and in transfected HEK293 cells that co-express SorCS2 and PGRN, the two proteins co-localized in
371 structures compatible with TGN and sorting vesicles. Interestingly, by immunoprecipitation
372 experiments we found that specifically the proform of SorCS2, which is enriched in the TGN, could
373 bind PGRN in a *cis*-configuration and prevent its secretion. As total PGRN levels were decreased too
374 when co-expressed in the HEK293 cells and PGRN was increased in spinal cords from *Sorcs2*$^{-/-}$ mice,
375 it is possible that SorCS2 may also traffic PGRN from the TGN to lysosomes for degradation or
376 processing into granulins. Notably, a similar complexity in function has also been reported for
377 sortilin. At the plasma membrane sortilin enables proNGF/proBDNF signaling, whereas in the TGN
378 it controls trafficking of BDNF to the regulated secretory pathway as well as to lysosomes for
379 degradation[12,60–62]. Future studies should address the cell biological mechanisms by which SorCS2
380 controls PGRN sorting and signaling from the plasma membrane.

381 In conclusion we have identified SorCS2 as a novel PGRN receptor required for motor neuron
382 outgrowth *in vivo* and *in vitro*. At the plasma membrane, SorCS2 enables PGRN signaling whereas
383 inside the cell it controls PGRN secretion and thereby its extracellular bioavailability. SorCS2 is
384 expressed in several neuronal subtypes and it is intriguing to speculate that the receptor is used more
385 broadly to transduce trophic signals by PGRN and sustain neuronal integrity. Notably, SorCS2 is
386 abundant in the cortical pyramidal neurons that degenerate in patients with frontotemporal dementia
387 caused by *GRN* haploinsufficiency. We propose SorCS2 as a candidate target in development of
388 disease-modifying treatments for motor neuron diseases and potentially for other neurodegenerative
389 disorders.

390 # Materials & methods

391 ## Zebrafish husbandry

392 Zebrafish were maintained according to institutional and national guidelines under breeding permit,
393 2017-15-0202-00098, from the Danish Animal Experiments Inspectorate under the Ministry of
394 Justice. Zebrafish were kept at the facility at Molecular Biology and Genetics at Aarhus University
395 under standard conditions with feeding four times a day on a 14 h light/10 h dark cycle at 28.5 °C.
396 The AB strain obtained from the European Zebrafish resource Center was used to produce wildtype
397 embryos for microinjections, RNA isolation, IHC and ISH. Zebrafish with the mutant allele
398 *sorcs2*^{sa11642} with a nonsense mutation in *sorcs2* exon 10 was obtained from the Zebrafish Mutation
399 Project[63]. Genotyping of mutant fish was performed by isolating genomic DNA from adult fish by
400 swabbing[64] and running PCR using KOD HotStart polymerase (Novagen) following standard
401 protocol with 100 ng of DNA, 5% DMSO and primers 5'-TATGCACACCCTGATCTTATGG-3'
402 and 5'-CACACATACCTGGCTGTTGTTT-3'. Sequencing of PCR products at Eurofins Genomics
403 was used to detect the specific point mutation in the mutant line. For live-imaging and *in situ* HCR
404 the transgenic line *Tg(mnx1:GFP)*^{ml2} from Zebrafish International Resource Center expressing GFP
405 in the primary motor neurons was used. Embryos were collected after mating, staged by hpf[65], and
406 kept in E3 buffer (5 mM NaCl, 0.17 mM KCl, 0.33 mM $CaCl_2$, 0.33 mM $MgSO_4$, 0.001‰ methylene
407 blue, 2 mM Hepes, pH 7.0) at 28°C.

408 ## Zebrafish microinjections

409 A *sorcs2* targeted splice site-inhibiting MO (sMO) targeting the exon 2/intron 2 boundary
410 (AAATCTTCTGTCACTTACCTCCACA) and standard control MO (cMO) were obtained from
411 GeneTools, LLC. Given an injection volume of 5 nL, injection mixes were made with phenol red
412 (0.2% in 1 mM HEPES, pH7.5), 5 ng of p53 MO to avoid unspecific apoptotic effects[66], and either
413 5 ng of cMO or 3.7 ng of the sMO. For rescue experiments 500 pg/injection of human *SORCS2*
414 mRNA was injected together with sMO. Injections were performed under a microscope using a
415 pico-injector in embryos from the 1 to 4-cell stage. Human *SORCS2* mRNA was transcribed from a
416 pcDNA3.1/zeo-SorCS2A-P716 plasmid (provided by Peder S. Madsen, Aarhus Univeristy) with
417 mMessage mMachine T7 Transcription kit (Thermo Fisher) and purified with RNA MinElute kit
418 (Qiagen).

419

420 **RT-PCR**

421 RNA was purified from 30-50 embryos using RNeasy Mini Kit (Qiagen) and RT-PCR was performed
422 to detect *sorcs2* mRNA in wt embryos using the Titanium One-Step RT-PCR kit (Clontech) with
423 primers 5'-TTTTGCGCACCTGTACCCAGCTG-3' and 5'-TAACGCGCTCCTGAAGCAGAGTC-
424 3' for detection of mRNA after injection of different amounts of sMO and 5'-
425 TTTTGCGCACCTGTACCCAGCTGTGTT-3' and 5'-
426 TAACGCGCTCCTGAAGCAGAGTCCATT-3' for the different developmental stages.
427 As a reference, the *rpl13a* gene was used with primers 5'-TCTGGAGGACTGTAAGAGGTATGC-
428 3' and 5'-AGACGCACAATCTTGAGAGCAG-3'.

429 **Whole-mount zebrafish *in situ* hybridization**

430 Whole-mount *in situ* hybridization was carried out as previously described in the 2010-updated
431 version[67] with addition of 5% Dextran Sulphate sodium salt (Sigma) to the hybridization mixture[68].
432 The *sorcs2* probe was transcribed using the DIG RNA Labelling Kit (Roche) with a T7 polymerase
433 from a PCR fragment made with the following primers on embryonic cDNA (the T7 promotor
434 sequence is shown in bold): 5'-GAAGACGCTCATCATGGCAG-3' and
435 5'-**TAATACGACTCACTATAGGG**AATGAGGATGACGCTGCTGT-3'.
436 Stained embryos were stored in 75% glycerol and images acquired using an Olympus IX71
437 microscope with an Olympus DP71 camera. Horizontal sections were obtained by molding stained
438 embryos in Tissue-TEK O.C.T. (Sakura) on dry ice and sectioning on a Microm HM 560 cryostat.

439 **Whole-mount zebrafish immunohistochemistry**

440 Whole-mount IHC was performed according to the protocol by GeneTex (www.genetex.com) with
441 minor modifications. Zebrafish embryos of the specified stage were dechorionated using sharp
442 forceps and fixated in 4% PFA ON at 4°C. Embryos were dehydrated and permeabilized according
443 to protocol, but blocked with PBS + 0.1% Tween20 + 10% goat serum 1h at 4°C. They were incubated
444 with znp-1 (1,25 µg/mL) in 0.1M potassium phosphate buffer (80% K_2HPO_4, 20% KH_2PO_4 + 0.8%
445 Triton X100) at 4°C 16-72h. Embryos were incubated with goat-anti-mouse 488 (1:1000, Thermo
446 Fisher) at RT 3h, immersed in 75% glycerol, and mounted laterally after removing the yolk sac[69].
447 They were imaged on a confocal laser-scanning microscope LSM-780 (Zeiss). For the motor axon
448 analysis, the 20X objective was used to obtain z-stacks with step intervals of less than 2.3 µm of
449 motor axons ranging from axon 5-16 counting rostrally. For analysis, each z-stack was split into the

450 two hemi-segments of the axon rows and z-projected using ImageJ software[70]. The axons were scored
451 using definitions described in [71] for length and [72] for branching.

452 For double staining of motor axons and AChRs, znp-1 and α-Bungarotoxin (BTX) were used with a
453 modified protocol from Bio-protocol[73]. After ON fixation, embryos were washed with PBS and
454 digested with 0.1% collagenase (1 mg/mL, Sigma) diluted in PBS with Ca^{2+} at RT 9 min for 27 hpf
455 embryos and 45 min for 48 hpf. Embryos were incubated 30 min at RT with α-BTX-555 (10 µg/mL,
456 Thermo Fisher) in PBT + 0.5% Triton X-100 + 10% NGS + 1% DMSO. They were then incubated
457 with znp-1 antibody and secondary antibody as described.

458 **Whole-mount zebrafish third generation *in situ* hybridization chain reaction**

459 *In situ* HCR v3.0[34] was performed with probes and reagents provided by Molecular Instruments
460 following their protocol. Zebrafish embryos were collected at 24, 27, and 48 hpf and fixated with 4%
461 PFA ON at 4°C. 48 hpf embryos were furthermore bleached 1 h with 3% H_2O_2/0.5% KOH/PBS
462 before dehydration to remove pigmentation. Following rehydration, the 48 hpf embryos were then
463 treated with Proteinase K for 20 min at RT and postfixated 20 min RT. All embryos were incubated
464 with 5 pmol/µl of probes ON at 37°C and hairpins as instructed. Two set of probes for *sorcs2* and
465 *grna* were used to increase signal. After washing, embryos were mounted laterally with Prolong Glass
466 Antifade Mountant (Thermo Fisher Scientific, P36984) after removing the yolk sac[69]. 10 µm cross
467 sections were obtained of zebrafish trunk by molding stained embryos in O.C.T. on dry ice and
468 sectioning on a Cryostar NX70. They were imaged on a confocal laser-scanning microscope LSM-
469 780 (Zeiss). A 20X objective was used to obtain z-stacks with step intervals of 1.9 µm of trunk motor
470 axons and cross sections. Z-stacks were z-projected for visualization using ImageJ software ensuring
471 correct representation of co-localization with volume of projection listed in figure legends.

472 **Zebrafish live-imaging**

473 cMO- and sMO-injected *Tg(mnx1:GFP)^{ml2}* embryos were dechorionated and anesthetized with
474 0.05% tricaine in E3 buffer. They were laterally molded at 18 hpf into 0.5% low-melt agarose in an
475 imaging dish with glass bottom and covered with E3 buffer containing tricaine to keep them sedated
476 during imaging. Embryos were imaged from 19 hpf until 39 hpf with a Nikon T*i* Eclipse automated
477 TIRF microscope equipped with a 10x differential interference contrast (DIC) air objective, a Perfect
478 Focus 3 system and a Zyla sCMOS5.5 Megapixel camera (Andor) controlled by NIS Elements
479 software from Nikon. The fluorescence illumination system was Cool LED-pE-300 white, and the

480 fluorescence filter set used was standard GFP. Imaging, using widefield settings, was performed
481 every 15 min for 20 h with 13 z-stacks separated with steps of 6 µm of both DIC light microscopy
482 and fluorescence microscopy. Images and videos were analysed using NIS Elements and ImageJ
483 software.

484 **Touch response assay for 48 hpf zebrafish embryos**

485 48 hpf cMO and sMO embryos were dechorionated and returned to incubator for least an hour to
486 avoid stress. In a petri dish with warmed E3, embryos were placed, one at a time, in the centre of
487 concentric circles drawn with an increase in diameter of 0.5 cm and touched with an embryo poker[69]
488 at the back from behind. Using a Zeiss axio zoom V16 microscope with a Hamamatsu high speed
489 camera, embryos were recorded for 10s collecting 100 images/s. Images were analysed using the
490 Hokawo software (Hamamatsu) and time spent swimming 1 cm determined. Embryos that did not
491 swim 1 cm or more were not included in analysis.

492 **List of primary antibodies**

Antibody	Source	IF	IF cells	Immunoblotting
β-actin	A5441 Sigma, mouse			1:5000
ChAT	AB144P Merck Millipore, goat	1:500	1:1000	
Foxp1	Gift from J. Dasen	1:1000		
GAPDH	Cell Signaling Technology			1:3000
GFP	Ab290 Abcam, rabbit	1:1000		
HA	18181 Abcam, mouse		1:500	
HA	H6908 Sigma, rabbit			1:500
Hb9	Gift from J. Dasen	1:1600		
Iba-1	#019-19741 Wako	1:500		
Progranulin	AF2420 R&D, goat		1:500	1:500
Progranulin	MAB24201 R&D, mouse			1:500 (Fig. 8H + S5)
Progranulin	AF2557 R&D, sheep	1:250		1:1000 (Fig. S2E)
SM1-32 (neurofilament H)	Biolegend, mouse	1:200		
SorCS2	AF4237 R&D, sheep	1:250 1:500 (E12.5)		1:1000
SorCS2	F7100 Dako custom-made, rabbit		1:2000	1:2000
Tuj1	MMS-435P Biosite, mouse		1:1000	

493

494 **Mouse background and breeding**

495 Animal studies were conducted with C57BL/6j BomTac wt mice (Taconic), *Sorcs2*$^{-/-}$ mice[13], and
496 B6.Cg-Tg(Hlxb9-GFP)1Tmj/J (*Hb9::GFP)* mice (Jackson Laboratories). Animals were bred at the
497 Animal Facility at Biomedicine Aarhus University, and experiments were approved by the Danish
498 Animal Experiments Inspectorate under permit 2016-15-0202-00051 and carried out according to
499 institutional and national guidelines. Animals were housed in the animal facility at Aarhus University

500 with light-dark cycles of 12h with light from 6 a.m. to 6 p.m. They were fed standard chow and water
501 *ad libitum* and their cages were cleaned every week and supplied with nesting, bedding material, and
502 a tunnel.

503 **Section preparation and immunohistochemistry of mouse embryos**

504 The protocol was kindly provided by Jeremy Dasen, NYU Langone, New York. E12.5 embryos were
505 beheaded and eviscerated before being fixated in 4% PFA for 1h 30 min. Tissue was subsequently
506 washed with PBS and kept in 30% sucrose ON at 4°C. Embryos were embedded in Tissue-TEK
507 O.C.T. and 10 µm sections cut on a cryostat (Cryostar NX70). Please note that we used RNA scope
508 sample preparation protocol prior to the IF of PGRN in E12.5 mouse embryos because it provided
509 staining of higher quality in case of this specific antibody.

510 Slides were washed with PBS to remove O.C.T. They were blocked 20 min with PBS + 0.1% Triton
511 X-100 + 1% BSA and incubated ON at 4°C with primary antibodies in blocking solution. Slides were
512 washed with PBS + 0.1% Triton X-100 and incubated 60 min at RT with secondary antibodies
513 (Jackson ImmunoResearch, Thermo Fisher) diluted 1:1000 in PBS + 0.1% Triton X-100. Mounted
514 with Vectashield (Vector Lab) and imaged on a confocal laser-scanning microscope LSM 700 (Zeiss).

515 **Fluorescent RNA scope *in situ* hybridization**

516 E12.5 mouse embryos were rinsed in PBS-pH7.4 (Invitrogen), and fixed in 4% PFA (Acros Organics)
517 at 4°C for 24 hours. The tissue was gradually immersed in 10%, 20%, and 30% of sacharose/PBS-
518 pH7.4 solution at 4°C until dehydrated. The embryos were washed, embedded in Tissue-TEK O.C.T.
519 (Sakura), and frozen to -80°C. The tissue was cryo-sectioned (Cryostar NX70) as 14 µm slices that
520 were air-dried in -20°C for 2 hours, and later stored at -80°C.

521 For the ISH, we implemented manufacturer instructions for fixed-frozen samples and RNAscope
522 Multiplex Fluorescent Reagent Kit v2 kit (ACD Biotechne, #323100) using the following probes:
523 Mm-Sorcs2-C1 (ACD Biotechne, #473411-C1) and Mn-Granulin-C3 (ACD Biotechne, #422861-
524 C3). For the fluorescent labeling, we used Opal-690 reagent pack (Akoya Biosciences,
525 FP1497001KT, 1:750) for the C1 probe, and Opal-570 reagent pack (Akoya Biosciences,
526 #FP1488001KT, 1:2000) for the C3 probe. To secure good Hb9-GFP signal, we subsequently
527 incubated the slides with rabbit anti-GFP antibody (Abcam, #ab290, 1:1000) in PBTA solution (0.3%
528 Triton X-100, 0.1% BSA, 5% donkey serum) at 4°C ON. The next day, we used secondary antibody
529 anti-rabbit Alexa-488 (Invitrogen, #A11008, 1:1000) together with Hoechst (Thermo Fisher

530 Scientific, #33342, 1:2000) for 1h in RT. We mounted the slides with Prolong Gold Antifade
531 Mountant (Thermo Fisher Scientific, #33342), and imaged them using confocal laser-scanning
532 microscope Zeiss LSM 800.

533 **Section preparation and immunohistochemistry of postnatal day 3 and adult spinal cord**

534 To preserve tissue morphology for IHC, transcardial perfusion fixation was performed on adult wt
535 and *Sorcs2*$^{-/-}$ mice, and spinal cords were dissected out and post-fixated in 4% PFA for 2-6 h. For P3,
536 the spinal cords with surrounding vertebrates were dissected from *Hb9::GFP* mice and fixated in 4%
537 PFA ON at 4°C. For both ages, the spinal cords were dehydrated in 30% sucrose ON at 4°C before
538 freezing in Tissue-TEK O.C.T. on dry ice. 40 µm sections of adult tissue were cut on a Microm HM
539 560 cryostat and 10 µm sections of P3 on a Cryostar NX70, and they were stored at -80°C until further
540 use.

541 For IHC staining slides were thawed and antigen-retrieval performed by incubating the sections with
542 preheated Target Retrieval Solution (DAKO) 20 min at 70°C. Sections were incubated in Tris-
543 buffered saline (TBS) + 5% donkey serum + 1% bovine serum albumin + 0.3% Triton X-100 for 30
544 min at RT for permeabilization of cells and blocking. Slides were incubated with primary antibodies
545 ON at 4°C. The subsequent day, the sections were washed with TBS + 0.05% Triton X-100 and
546 incubated with secondary antibodies (1:300, Thermo Fisher) 4h at RT. After incubation with Hoechst
547 (0.2 µg/mL, Thermo), the slides were mounted using DAKO mounting medium. Images were
548 acquired on a confocal laser-scanning microscope LSM-780 (Zeiss).

549 **Whole-mount immunostaining of mouse embryos**

550 For whole-mount staining of embryonic motor nerves, heterozygous *Hb9::GFP* mice expressing GFP
551 under the *Mnx* promotor were crossed with *Sorcs2*$^{-/-}$ or wt mice. The mice display GFP expression in
552 dendrites, axons and soma of spinal motor neurons from E9.5 to P10. Embryos were collected at
553 E12.5 and stained as demonstrated in [74]. In brief, embryos were beheaded, eviscerated and pinned
554 down on a silicone plate on ice with limbs slightly stretched out. Embryos were fixated ON at 4°C
555 with 4% PFA. The embryos were then bleached 4h at 4°C with Dent's bleach (1 part H_2O_2 : 2 parts
556 Dent's fix) followed by ON-fix with Dent's fix (1 part DMSO : 4 parts MeOH). After washing with
557 PBS, embryos were incubated in blocking solution consisting of PBS + 0.5% BSA + 20% DMSO 30
558 min at RT. Embryos were transferred to anti-GFP diluted in blocking solution 3 days ON gently
559 rocking at RT. Embryos were then washed with PBS and incubated with donkey-anti-rabbit-488

560 (1:1000, Thermo Fisher) in blocking solution ON at RT. Following washes with PBS and MeOH,
561 embryos were cleared with BABB (1 part benzyl alcohol : 2 parts benzyl benzoate). GFP-labelled
562 motor axons were visualised in confocal z-stacks (around 400 µm thick) using a confocal laser-
563 scanning microscope LSM-780 (Zeiss) and analysed using ImageJ software.

564 **Surface plasmon resonance analysis**

565 Surface plasmon resonance was performed to assess protein-protein interaction and determine
566 binding affinity on a Biacore 3000 instrument. Soluble SorCS2 was immobilized at a density of
567 0.0862 pmol/mm^2 on a CM5 sensor chip. hPGRN was dialysed against 10 mM HEPES (pH 7.4), 150
568 mM NaCl, 1.5 mM CaCl2, 1 mM EGTA, and 0.005% surfactant P20 (running buffer), and 25–250
569 nM of the ligand was injected (5 ml/min) through the flow cell at 20°C. After 600 s, running buffer
570 containing PGRN was substituted with buffer lacking the ligand, allowing for determination of both
571 the association and dissociation constants. The binding response is expressed in relative response
572 units, i.e., the difference in response between the immobilized protein flow cell and a corresponding
573 control flow cell. Kinetic parameters were determined using the BIAevaluation 3.0 software.

574 **Primary motor neuron cultures**

575 Primary motor neurons were prepared from E13.5 mice embryos as described in [42] with minor
576 modifications. Panning plates were coated with monoclonal anti-murine p75^{NTR} antibody (1,46
577 µg/mL, Ab8877 Abcam) ON at 4°C diluted in sterile 10 mM Tris-HCl pH 9.5. Isolated motor neurons
578 were counted with Neubauer counting chambers and seeded on Poly-DL-ornithine hydrobromide-
579 (PORN, Sigma) and Laminin (Invitrogen)-coated coverslips in complete medium (Neurobasal
580 medium supplemented with GlutaMax I, senicillin/streptomycin (1:100, Gibco), B27 (2%,
581 Invitrogen), 2% horse serum). Cells were cultured at 5% CO_2 and 37°C. On day 1 and 3, 80% of
582 complete medium was changed to either new complete medium without trophic factors or complete
583 medium containing 5 ng/mL BDNF (GF029 Merck Millipore) or 100 ng/mL human PGRN (AG-
584 40A-0188Y Adipogen). On day 4, the cultures on coverslips were fixated with 4% PFA for 20 min,
585 washed and stored in PBS at 4°C until immunostaining.

586 **Immunostaining of primary motor neurons and analysis**

587 For immunostaining of the primary motor neurons, coverslips with neurons were permeabilized in
588 PBS + 0.1% Triton X-100, blocked with PBS + 10% fetal bovine serum (FBS) 30 min at RT, and
589 incubated with primary antibodies ChAT or Tuj1 (neuronal class III β-tubulin) diluted in blocking

590 solution ON at 4°C. After washing, coverslips were incubated with secondary antibodies 2h at RT
591 and nuclei stained with Hoechst (0.2 µg/mL). Coverslips were mounted with DAKO mounting
592 medium and imaged using an Apotome 2.0 microscope (Zeiss). Neurons were measured using
593 ImageJ, and neurites longer than twice the length of the soma and projecting directly from the cell
594 body were considered primary. Secondary neurites were defined as neurites protruding from the
595 primary, and tertiary as neurites protruding from the secondary. 31-39 neurons of each genotype and
596 stimulation were analyzed from two independent experiments.

597 **Mouse RT-qPCR**

598 Cortex, hippocampus, cerebellum, spinal cord and gastrocnemius muscle from wt and *Sorcs2*$^{-/-}$ mice
599 were collected in RNAlater (Invitrogen) and left ON at 4°C. The following day the tissue was lysed
600 in RLT buffer and RNA purified using RNeasy (Qiagen). cDNA was synthesized using the High
601 Capacity RNA-to-cDNA kit (Thermo Fisher). RT-qPCR was performed using TaqMan Fast
602 Advanced Master Mix (Applied Biosystems), TaqMan expression probes, and a 7500 Fast Real-Time
603 PCR system (Thermo Fisher). *Hprt* and *Gapdh*, were used for normalization measuring fold change
604 by $2^{-\Delta\Delta Ct}$, and three technical and three biological replicates were analyzed. All TaqMan probes
605 were determined to be within 90-110% efficiency. TaqMan probes used (Thermo Fisher): *Sorcs2*
606 (Mm00473050_m1), *Grn* (Mm00433848_m1), *Gapdh* (Mm99999915_g1), *Hprt*
607 (Mm00446968_m1).

608 **Immunoblotting**

609 Spinal cords from wt and *Sorcs2*$^{-/-}$ mice were dissected and lysed on ice with TNE lysis buffer (Tris-
610 base 10 mM, NaCl 150 mM, EDTA 1 mM, NP40 1%, cOmplete 1% (Roche), PhosSTOP 1%
611 (Roche)) and mechanically with a pellet pestle. Lysed tissue was centrifuged at 13,000 rpm and
612 protein concentration of the supernatant measured using a bicinchoninic acid assay. Protein samples
613 were denatured by boiling with SDS sample buffer and 20 mM DTT. Proteins were then separated
614 by SDS-PAGE using a precast NuPAGE 4-12% Bis-Tris Gel (Invitrogen) and transferred to an PVDF
615 membrane by immunoblotting in blotting buffer (192 mM glycine, 25 mM Tris-Base, pH 8.0). The
616 membrane was subsequently blocked in 0.05 M Tris-base, 0.5 M NaCl, 0.1% Tween-20 (TST buffer)
617 + 2% skimmed milk powder and 0.5% Tween-20 and washed in wash buffer (10 mM HEPES pH 7.8,
618 140 mM NaCl, 2 mM CaCl2, 1 mM mgCl2, 0.2% skimmed milk powder, 0.05% Tween-20). It was
619 incubated with primary antibodies diluted in wash buffer for 2h at RT, then HRP-conjugated

620 secondary antibodies (DAKO) and visualized with chemiluminescence using ECL Western Blotting
621 Detection Reagents (GE Healthcare) and the imaging system FUJI Film LAS 4000 (GE Healthcare).

622 **Facial nerve crush injury**

623 The facial nerve crush surgery was performed at VIB-KU Leuven and were approved by Institutional
624 Animal Care and Ethical Research Advisory Committee of the University of Leuven, Belgium
625 (P132/2012 and P015/2015). The surgeries were performed as described previously[27] on 10 weeks
626 old wt and *Sorcs2*$^{-/-}$ mice of both sexes that were shipped to Belgium from Denmark. To evaluate
627 regeneration of facial nerve axons, all mice were examined twice daily (9-10 am and 6-7 pm) for
628 whisker movement. Whisker movement scores were given according to the following scale: 0 for no
629 detectable movement, 1 for detectable motion of individual whiskers, 2 for significant (but
630 asymmetric) voluntary motion, and 3 for symmetric voluntary motion. The contralateral whiskers
631 were used as a reference for complete functional recovery.

632 Immunostaining of the facial motor nucleus was performed as described previously[27]. Images were
633 acquired using a Leica SP8x confocal microscope.

634 **Cell cultures, transfection and co-cultures**

635 Human embryonic kidney 293 cells (HEK293, ATCC) were grown at 37°C with constant 95% of
636 H_2O and 5% of O_2. Cells were cultivated in Dulbecco's Modified Eagle's medium (DMEM, Sigma)
637 supplemented with 10% FBS and 50 U/ml penicillin/streptomycin (all Thermo). Cells were
638 trypsinized in 1 ml of Trypsin_0.05%-EDTA (Thermo) and seeded into 10 cm dishes in 40%
639 confluence 24 hours prior the experiment. The next day, the cells were transfected using FuGENE 6
640 transfection reagent (Promega). Transfection mixture was prepared in serum-reduced OptiMEM
641 medium (Thermo) using 6 µg of plasmid DNA per dish (3 µg DNA1 : 3 µg DNA2). The following
642 plasmid DNAs were used in this study: pcDNA3.1, pcDNA3.1-human_SorCS2_Full length,
643 pCMV3-human_Progranulin (Sino Biological, #HG10826-UT) and pCMV3-HA-
644 human_Progranulin (Sino Biological, # HG10826-NY). Transfection mixture was added to 7 ml of
645 complete cell media and incubated for 24 hours. 24 hours post transfection, cells were trypsinized in
646 1 ml of trypsin and seeded into either 10 cm dishes for co-IP experiments (8 ml of fresh media plus
647 400 µl of cell suspension, or 400 µl + 400 µl of cell suspension for the co-cultures), or into 24-well
648 plates that contained glass cover-slips coated with Poly-L-Lysine. For the coverslips, 3.5 ml of fresh
649 media with 100 µl cell suspension was added for single-transfections, or 50 µl + 50 µl for the co

650 cultures. 500 µl of this mixture was seeded per well. The cells were subsequently grown 24h and
651 harvested 48h post transfection.

652 **Co-immunoprecipitation and immunoblotting**

653 For the co-IP experiments, HEK293 cells were harvested either 24 or 48h post transfection. First, 2
654 ml of cell media was spun down at 200g for 5 min at RT to remove the cell debris. The samples were
655 placed on ice and cells were washed with PBS, before adding 1 ml of TNE lysis buffer while shaking
656 at 4°C for 20 min. Cell lysates and cell medium were spun down at 20,000g at 4°C for 15 min, and
657 supernatant was kept for further processing. 60 µl from each sample was used as an INPUT reference
658 sample and was mixed with 20 mM DTT and NuPAGE LDS sample buffer. 400-600 µl of the cell
659 lysate per condition were used for the pulldown. The following antibodies were used: 1µg of
660 progranulin (AF2420 R&D), 1.5 µg of rabbit anti-HA (H6908 Sigma), and 1 µg of mouse-anti-HA
661 (26183 Sigma). Cell lysates were incubated with antibodies for 14-16h in 4°C. Meanwhile, 30 µl
662 GammaBind G Sepharose beads (Sigma) per sample were washed with PBS, centrifuged at 300g for
663 5 min at RT, and washed in TNE lysis buffer before another centrifugation step at 300g for 5 min at
664 RT. Washed beads were incubated with the antibody-lysate for 4h at 4°C with slow rotation. Samples
665 were subsequently washed on ice with PBS + 0.1% Tween20 and spun down at 200g for 1 min at
666 4°C. Proteins were eluted by heat in elution buffer (TNE buffer, 20 mM DTT, NuPAGE LDS sample
667 buffer). All the samples (including INPUT) were immediately boiled at 95°C for 5 minutes and
668 subjected to immunoblotting using home-made 8% Tris-Glycin polyacrylamide SDS-Page gels.

669 Immunoblotting was performed as described in previous section. Secondary antibodies fused with
670 HRP (DAKO) were used in dilution 1:2000. The immunoblots were developed dependent on the
671 strength of the signal either with ECL Amersham RPN2106 (Sigma) or Immobilon Forte Western
672 HRP substrate (Sigma). Images were processed using Adobe Photoshop CC. Band intensity was
673 measured in ImageJ and analysed in Microsoft Excel. The band intensities of IB: PGRN and IB: HA
674 were further normalized to the band intensity of β-actin (loading control). To describe relative band
675 intensity, the values were further normalized to IB of Progranulin single transfection, which was set
676 as 1.

677 **Immunostaining of HEK293 cells**

678 Transfected HEK293 cells were harvested for immunofluorescence 48h post transfection. They were
679 fixated with 4% PFA at RT for 15 min. Immunofluorescence was performed as described
680 previously[75]. Secondary antibodies (Thermo) were used in dilution 1:800 for 1h at RT. The samples

681 were imaged using scanning confocal microscopy system Zeiss LSM-780. The images were
682 processed in Adobe Photoshop CC.

683 **Statistical analysis**

684 Student's T-test was used to compare differences in mean between two groups. Mann-Whitney test
685 was used to compare ranks between non-normal distributed data. For multiple comparisons within
686 the same experiment the Holm-Šídák method was used to correct for multiple comparisons with α =
687 0.05 unless otherwise stated. For analysis of more than two groups, analysis of variance (ANOVA)
688 was performed followed by Tukey's multiple comparison test for comparing every mean with every
689 other mean or Dunnett's for comparing every mean with a control mean. Repeated measures two-
690 way ANOVA with Šídák correction was used for the analysis of facial nerve recovery since values
691 were matched according to time. All statistics was performed using the GraphPad Prism software. A
692 p-value of < 0.05 was considered statistically significant. Data are presented as mean (standard error
693 of mean, s.e.m.) unless otherwise stated.

694 **Analysis of deposited RNA sequencing data**

695 The single-cell transcriptome atlas of zebrafish embryos[35] on http://zebrafish-dev.cells.ucsc.edu was
696 used to assess expression of *sorcs2* and *grna,*.

697 Transcriptional data from laser-captured motor neurons from the spinal cord, the facial nucleus, and
698 the cranial nuclei 3 and 4[46] was downloaded from NCBI Gene Expression Omnibus (GEO)
699 (GSE115706), and normalized expression values (RPKM) extracted and plotted for *Sorcs2* and *Grn*.

700

701 ## Acknowledgements

702 We wish to thank the entire Nykjaer laboratory for helpful discussions. Benedicte Vestergaard,
703 Andreea-Cornelia Udrea, Anja Aagaard, and Anne Kerstine Thomassen are thanked for excellent
704 technical assistance, and Peder S. Madsen for the SorCS2 plasmid. Thanks to Petra Kompanikova
705 who helped establish the *in situ* HCR v3.0. PBT sends her gratitude to Moses Chao and his group for
706 hosting her at NYU, and to Jeremy Dasen and his group members for all their help. The study was
707 funded by the Lundbeck Foundation (Grant Nos. R90-2011-7723, R248-2017-431, and R315-2018-
708 3066), The Danish National Research Foundation (Grant No. DNRF133), The Danish Council for
709 Independent Research (Grant No. 7016-00261), The Bluefield Project (Grant No. BFP-AN-2022),
710 EMBO (Grant No. 7375), and The Danish Society for Biochemistry and Molecular Biology. PVD

holds a senior clinical investigatorship of FWO-Vlaanderen and is supported by the E. von Behring Chair for Neuromuscular and Neurodegenerative Disorders, the ALS Liga België and the KU Leuven funds “Een Hart voor ALS”, “Laeversfonds voor ALS Onderzoek” and the “Valéry Perrier Race against ALS Fund”.

Author contributions

PBT performed the majority of experiments and data analysis and prepared the figures under supervision by AN. AS performed interaction studies (co-expression in HEK293 cells and IP) with help from PLO, analysis of murine RNA seq. data together with PQ, and IF of PGRN and RNA scope of *Grn* in E12.5 mice together with SN. AS helped prepare figures for the mentioned experiments. HL contributed to RT-PCR and prepared h*SORCS2* mRNA for rescue experiments. JTJ assisted with immunoblotting, in tissue collection, and in isolating, growing and staining primary motor neurons. SB performed the facial nerve crush and scored recovery together with PBT under supervision of PVD. JD provided mouse embryo sections, antibodies, and guidance for IF. Zebrafish studies were performed under supervision from KKS as well as HL, LNN, and CO. MVC contributed with scientific discussions and critical review of the manuscript. PBT, AS, and AN wrote the manuscript with input from all authors.

Competing interests

The authors declare no competing interests.

Figure 1

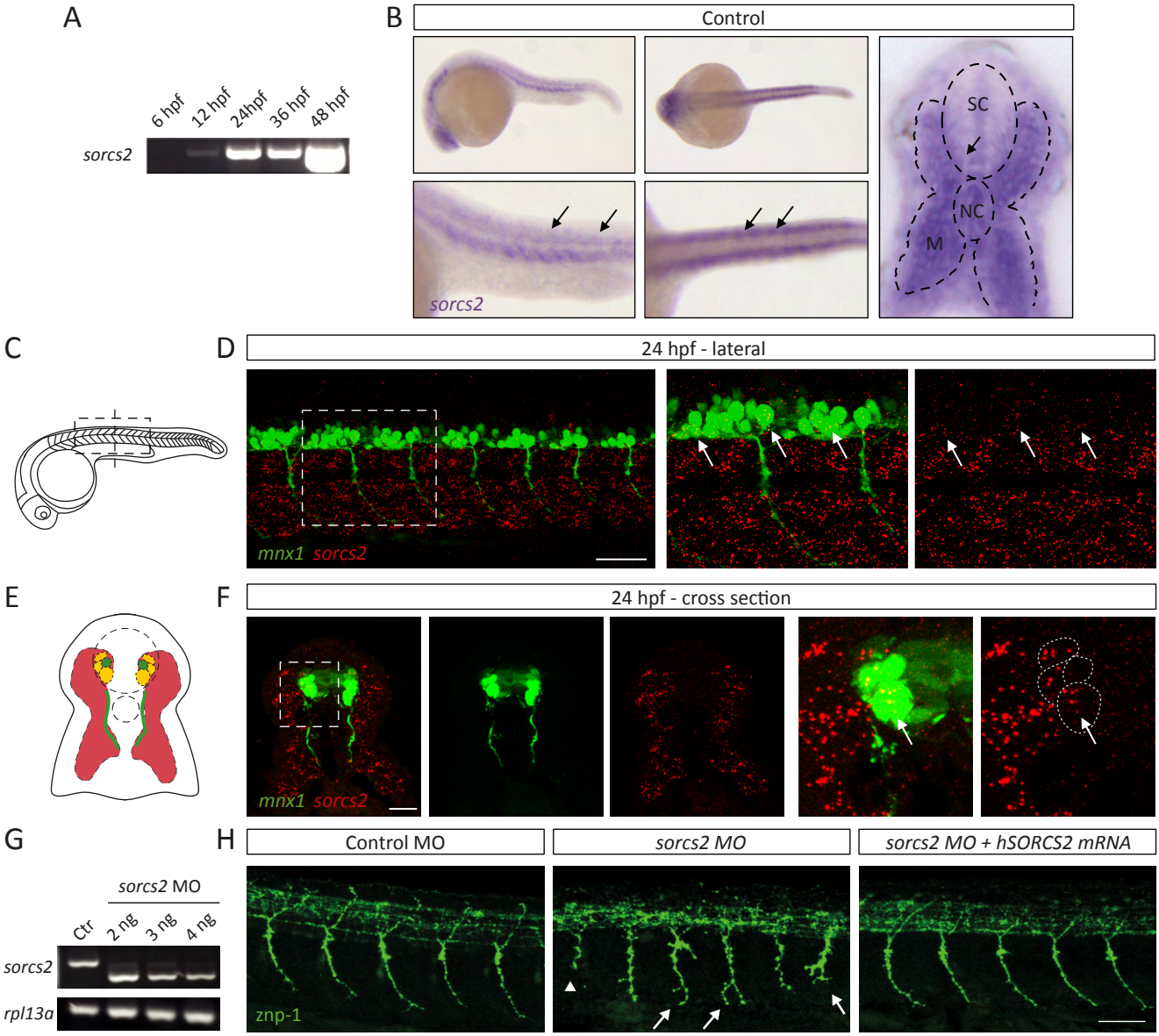

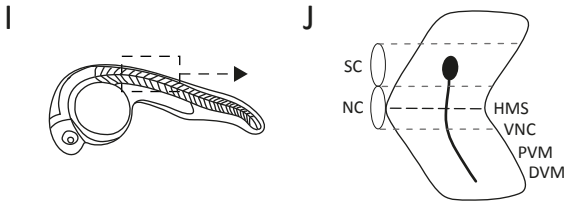

K

Branching	
Slight	One or more short fine projections along the axon.
Moderate	One or two slightly longer, thicker projections.
Severe	Several long projections or multiple (>2) branches, loops, early bifurcations ect.

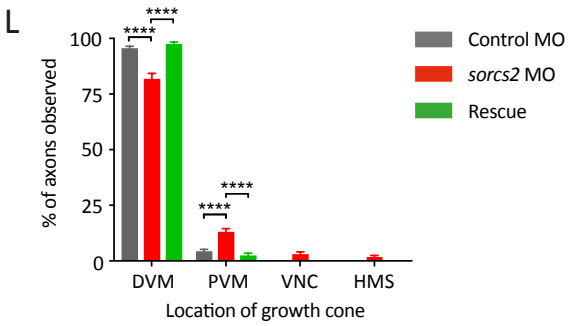

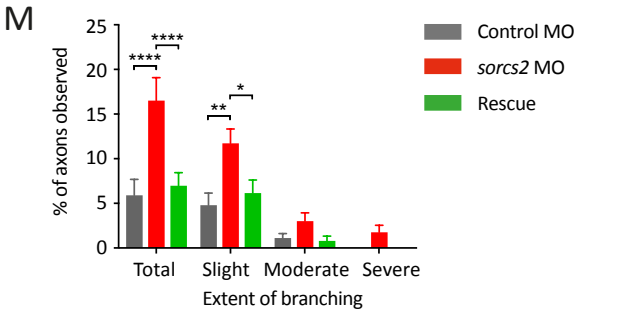

732 **Figure 1: *Sorcs2* knockdown causes stunted and aberrantly branched primary motor axons in zebrafish embryos**
733 **(A)** RT-PCR showing s*orcs2* is increasingly expressed from 12 hours post-fertilization (hpf). **(B)** I*n situ* hybridization
734 (ISH) of *sorcs2* at 24 hpf. Left; Lateral and dorsal view of control embryos showing staining in somites and ventral spinal
735 cord (SC) Right: cross section of control SC. Muscle (M) outlined with dashed lines. NC = notochord. Motor neurons are
736 indicated by arrows. **(C-F)** *In situ* HCR for *sorcs2* in *Tg(mnx1:GFP)*^{ml2} embryos at 24 hpf showing *sorcs2* in GFP+ motor
737 neurons (arrows) in lateral (C-D) and cross sectional (E-F) view. (**C**) Area studied in **(D**) is boxed**.** (**E**) Representation of
738 cross sections shown in (**F**). Images are z-projection of 4 µm (D) and 10 µm (F). Marked areas in D and F, left panels,
739 are enlarged in the corresponding right panels, scalebar = 50 µm for (D) and 20 µm for (F). **(G)** Efficacy of splice-site
740 inhibiting *sorcs2* morpholino (MO) injected at different dosages compared to 5 ng of control (ctr) MO assessed 24 hpf
741 by RT-PCR of *sorcs2* and the housekeeping gene, *rpl13a.* Injections made with 5 ng p53 MO. **(H)** Znp-1 immunostaining
742 showing abnormal length (arrowhead) and branching (arrows) of CaP axons in zebrafish treated with sMO compared to
743 control MO at 27 hpf. Rescue of phenotype by co-injection of sMO with h*SORCS2* mRNA. Scalebar = 50 µm. **(I)**
744 Representation of zebrafish embryo. The box shows area used for CaP analysis. **(J)** Model showing CaP projection into
745 four defined regions used for scoring axon outgrowth[71]. HMS, horizontal myoseptum; VNC, ventral edge of notochord;
746 PVM and DVM, distal and proximal ventral myotome. **(K)** Definitions for scoring branching[72]. Axon outgrowth **(L)** and
747 branching **(M)** in CaP from control MO (n = 21) and *sorcs2* MO zebrafish (n = 27), and following rescue (n = 18) are
748 shown in percentage. Error bars: s.e.m., n = number of embryos. P-value determined with two-way ANOVA and Tukey's
749 multiple comparisons. **** < 0.0001, ** < 0.01.
750

Figure 2

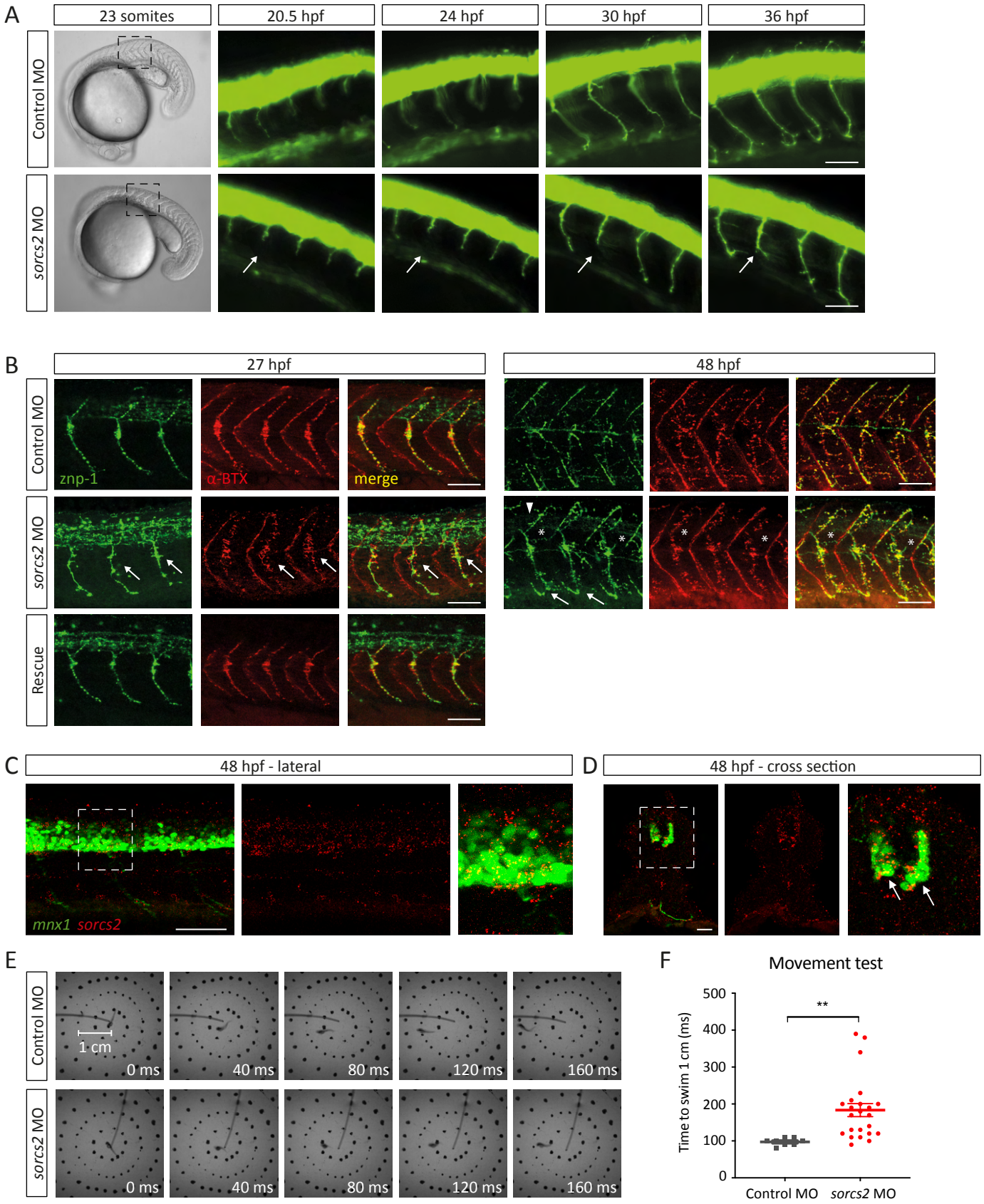
A
23 somites
20.5 hpf
24 hpf
30 hpf
36 hpf
Control MO
sorcs2 MO
B
27 hpf
48 hpf
Control MO
sorcs2 MO
Rescue
znp-1
α-BTX
merge
C
48 hpf - lateral
mnx1 sorcs2
D
48 hpf - cross section
E
Control MO
sorcs2 MO
1 cm
0 ms
40 ms
80 ms
120 ms
160 ms
F
Movement test
Time to swim 1 cm (ms)
500
400
300
200
100
0
**
Control MO
sorcs2 MO

751 **Figure 2: Neuromuscular defects and altered motility in *sorcs2* deficient embryos**

752 **(A)** Differential interference contrast images of 20.5 hpf embryos and time-lapse of control and *sorcs2* MO
753 *Tg(mnx1:GFP)*^{ml2} from 20.5-36 hpf (enlargement of black box). The white arrow shows a truncated axon, which pauses
754 longer at the first choice point (HMS) before continuing ventrally, yet remaining truncated at later stages. Scalebar = 20
755 μm. **(B)** Immunofluorescent staining of the NMJ. Lateral view of znp-1 (axons, green) and bungarotoxin (AChRs, red)
756 in control MO, *sorcs2* MO and rescue embryos at 27 hpf (left) and 48 hpf (right). At 27 hpf, AChR clusters are elongated,
757 diffuse and without complete co-localization with axons in *sorcs2* MO (arrows). At 48 hpf, axons in *sorcs2* KD embryos
758 have advanced less into the myosepta both at the ventral (arrows) and dorsal sides (arrow head, no innervation) and with
759 less co-localization between axon branches and AChRs in somite (asterisks). Scalebar = 50 μm. *In situ* HCR of 48 hpf
760 *Tg(mnx1:GFP)*^{ml2} embryos showing *sorcs2* in GFP+ motor neuron cell bodies with lateral view **(C)** and cross section **(D)**.
761 Images are z-projection of 16 μm (C) and 10 μm (D). Dashed squares are enlarged on the right side in each panel, scalebar
762 = 50 μm for (C) and 20 μm for (D). **(E)** Images show responses of 48 hpf control and *sorcs2* MO embryos to touch. The
763 distance between the center and second circle is 1 cm. **(F)** Time spent to swim 1 cm. *Sorcs2* MO embryos shows a
764 significantly slower escape response to touch. Error bars: s.e.m. within groups. P-value determined with student's t-test,
765 ** < 0.01.

766

Figure 3

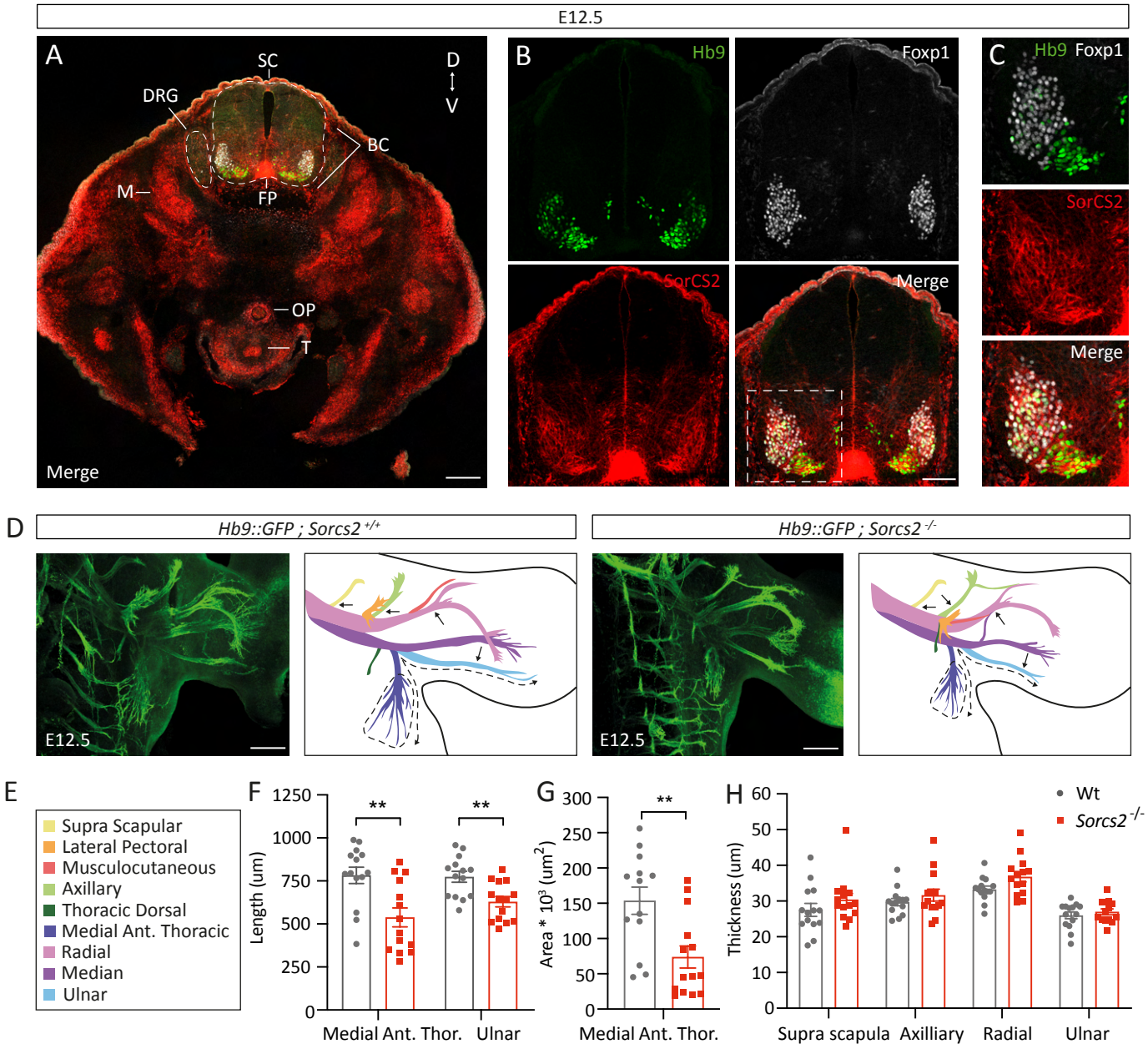

Figure 3: Perturbed motor axon outgrowth in *Sorcs2*$^{-/-}$ mice

(A-C) Immunofluorescent staining of SorCS2 (red) and motor neuronal transcription factors, Hb9 (green) and Foxp1 (white) in horizontal sections of E12.5 mice. SorCS2 is expressed in motor neurons, floor plate (FP), muscle (M), oesophagus (OE), trachea (T) and boundary cap (BC) cells, but not, or only very faintly, in dorsal root ganglia (DRG). Heart, lungs and intestines have been removed. D = dorsal, V = ventral. Scalebar = 200 µm in (A) and 50 µm in (B). **(C)** Enlargement of the area of interest boxed in (B) shows expression of SorCS2 in motor neurons of the ventral horn. **(D)** GFP fluorescence of whole-mount *Hb9::GFP* and *Sorcs2*$^{-/-}$;*Hb9::GFP* embryos at E12.5. Axon outgrowth is impaired in SorCS2-deficient embryos. Schematic representations of the innervation pattern with motor nerves color coded according to Catela *et al.* 2016[74]. Dashed lines indicate the area measured, and dashed arrows and arrows the nerves of which the length and diameter have been quantified, respectively. Scalebar = 200 µm. **(E)** Color-codes of the forelimb nerves. Quantification of nerve lengths **(F)**, the area covered by the medial anterior thoracic nerve **(G),** and the nerve diameters **(H)** for control and *Sorcs2*$^{-/-}$ embryos (n =14). Data shown as mean ± s.e.m. P-value determined with multiple t-test, Holm-Šídák corrected, or Mann-Whitney test for area spanned, ** < 0.01.

Figure 4

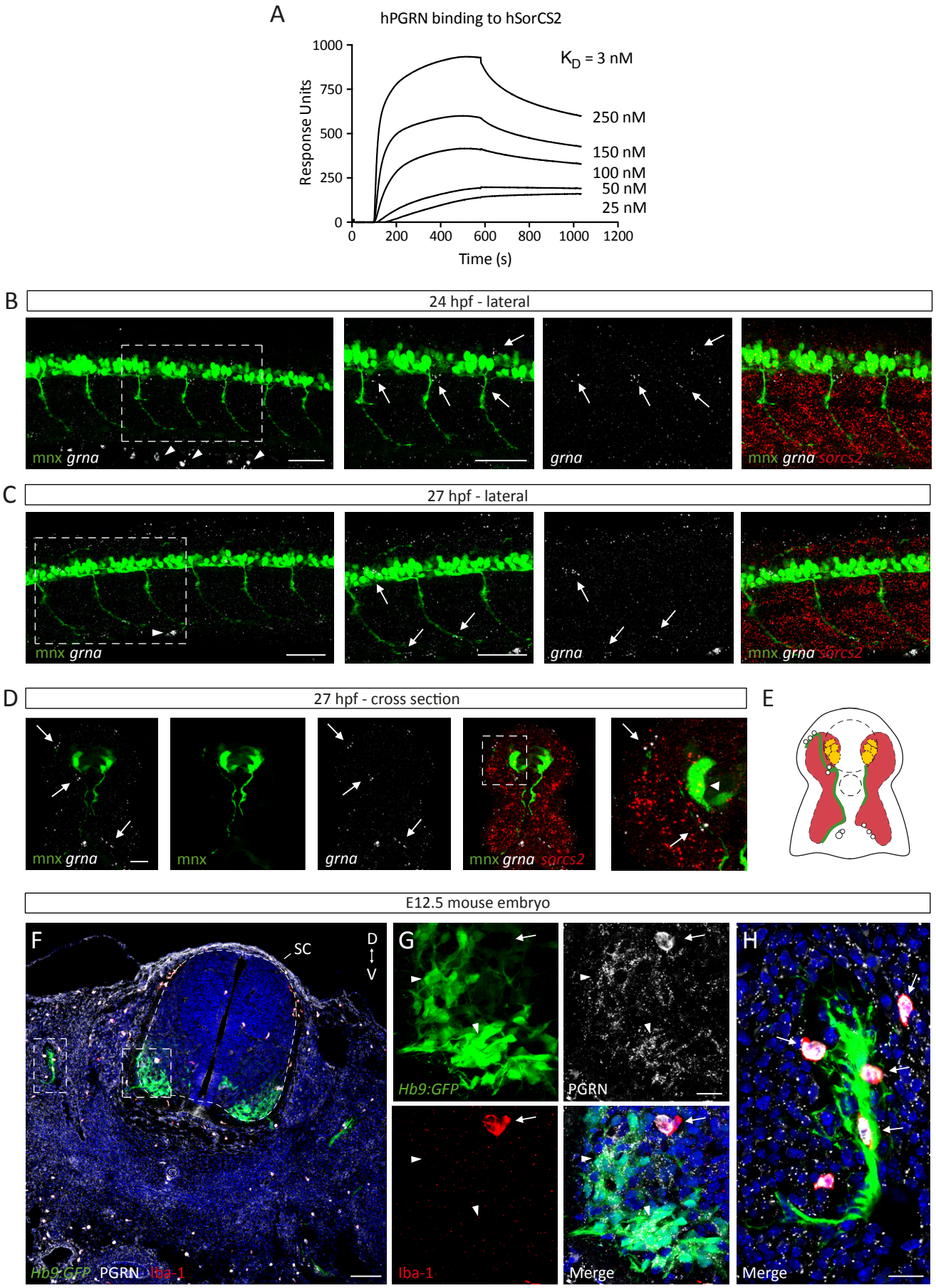
A
hPGRN binding to hSorCS2
Response Units
1000
750
500
250
0
0
200
400
600
800
1000
1200
Time (s)
K_D = 3 nM
250 nM
150 nM
100 nM
50 nM
25 nM
B
24 hpf - lateral
mnx grna
grna
mnx grna sorcs2
C
27 hpf - lateral
mnx grna
grna
mnx grna sorcs2
D
27 hpf - cross section
mnx grna
mnx
grna
mnx grna sorcs2
E
E12.5 mouse embryo
F
SC
D
V
Hb9:GFP PGRN Iba-1
G
Hb9:GFP
PGRN
Iba-1
Merge
H
Merge

Figure 4: Binding of progranulin to SorCS2 and expression in zebrafish and mice

(A) Concentration-dependent binding of hPGRN to immobilized SorCS2 (Kd = 3 nM) demonstrated by surface plasmon resonance analysis. *In situ* HCR on *Tg(mnx1:GFP)*^{ml2} embryos for *grna* shows expression along the yolk extension likely representing immune cells (arrow heads) and in close proximity to motor axons (arrows) at 24 **(B)** and 27 hpf **(C-D)**. Images are z-projection of 2 µm (B), 14 µm (C), and 10 µm (D). Dashed squares are enlarged to the right, scalebar = 50 µm for (B-C) and 20 µm for (D). **(E)** Schematic representation of a cross section of 27 hpf depicting *sorcs2* expression (red) in motor neuron cell bodies and skeletal muscle and *grna* (white) along extending motor axons (green). **(F-H)** Immunofluorescent staining of PGRN (white) and macrophage/microglia-marker, Iba-1 (red), in horizontal sections of E12.5 *Hb9::GFP* mice. **(F)** PGRN is expressed in scattered, brightly stained cells of which many co-express Iba-1 throughout the embryo. SC = spinal cord, V = ventral, D = dorsal. **(G)** Enlargement of ventral horn (white square) showing PGRN in Iba-1+ cells closely positioned to motor neurons (arrow), and PGRN expression in developing GFP+ motor neurons (arrow head). **(H)** Enlargement of projecting motor nerve (white rectangle) with PGRN in Iba-1+ cells (arrows) in close proximity to the motor axons (green). Nuclei are stained using Hoechst. Scalebar = 100 µm in (F) and 20 µm in (G-H).

Figure 5

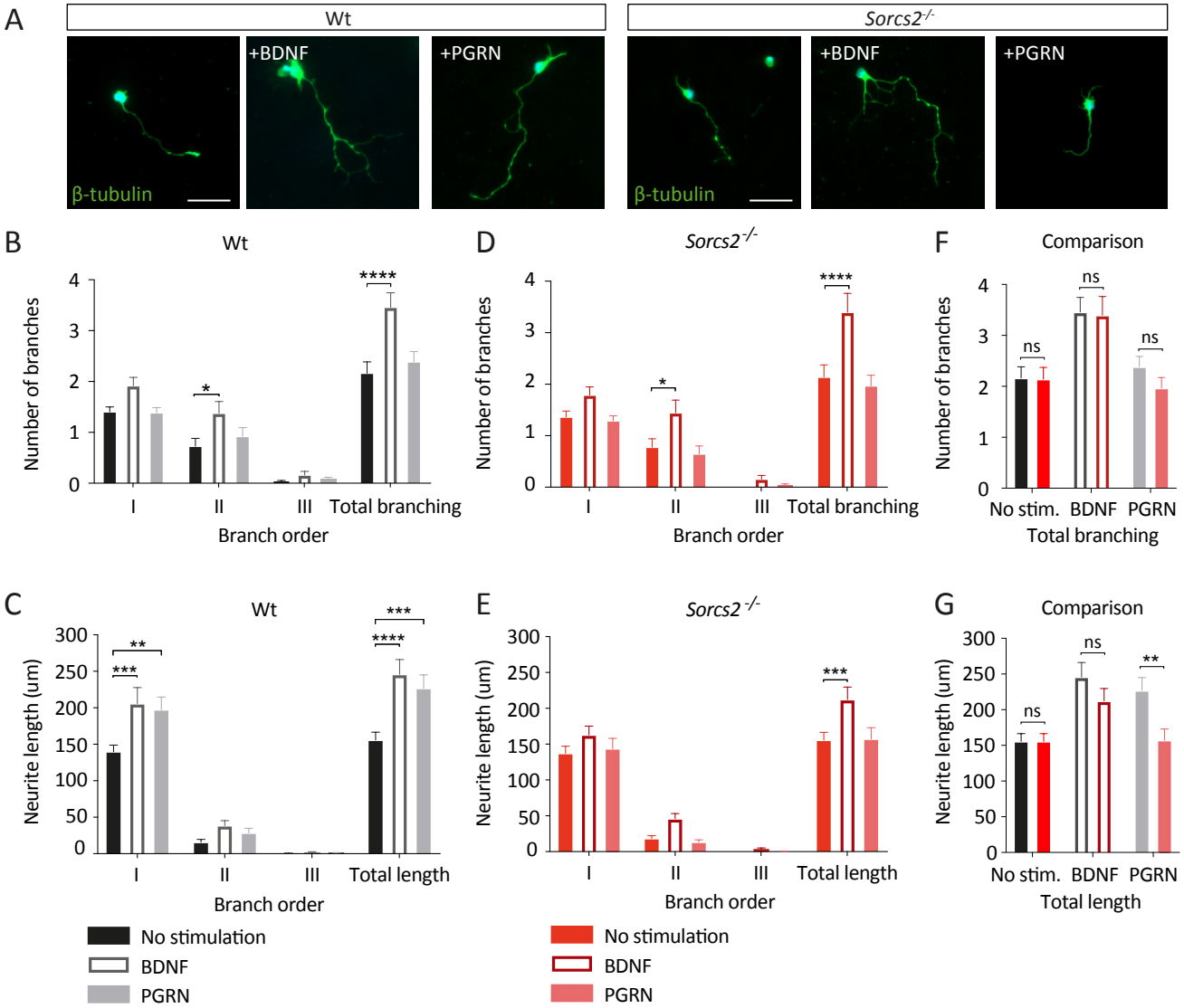

796 **Figure 5: PGRN-induced motor neurite outgrowth requires SorCS2 expression**

797 Primary motor neurons isolated from E13.5 murine spinal cord were cultured for 4 days. **(A)** Neurite outgrowth visualized
798 by β-tubulin staining (green) in representative wt and *Sorcs2*$^{-/-}$ motor neuron cultures grown either without stimulation,
799 with 5 ng/mL BDNF, or 100 ng/mL PGRN. Scalebar = 50 µm. Number of branches **(B+D)** and neurite length **(C+E)** of
800 primary, secondary, tertiary neurites. The total neurite length or branching are summarized for wt (grey tones) and *Sorcs2*$^{-}$
801 $^{/-}$ (red tones) motor neurons (Wt; no stim. = 37 neurons, BDNF = 37, PGRN = 39, *sorcs2*$^{-/-}$; no stim = 36, BDNF = 38,
802 PGRN = 31). Comparisons of total branching **(F)** and total neurite length **(G)** between genotypes show that only PGRN
803 stimulation of neurite outgrowth is significantly different between the two. Data shown as mean ± s.e.m. n = neurons. P-
804 value determined with two-way ANOVA and Dunnet's multiple comparisons test (C-E) or Šídák (F-G). * < 0.05, ** <
805 0.01, *** < 0.001, **** <0.0001.

806

Figure 6

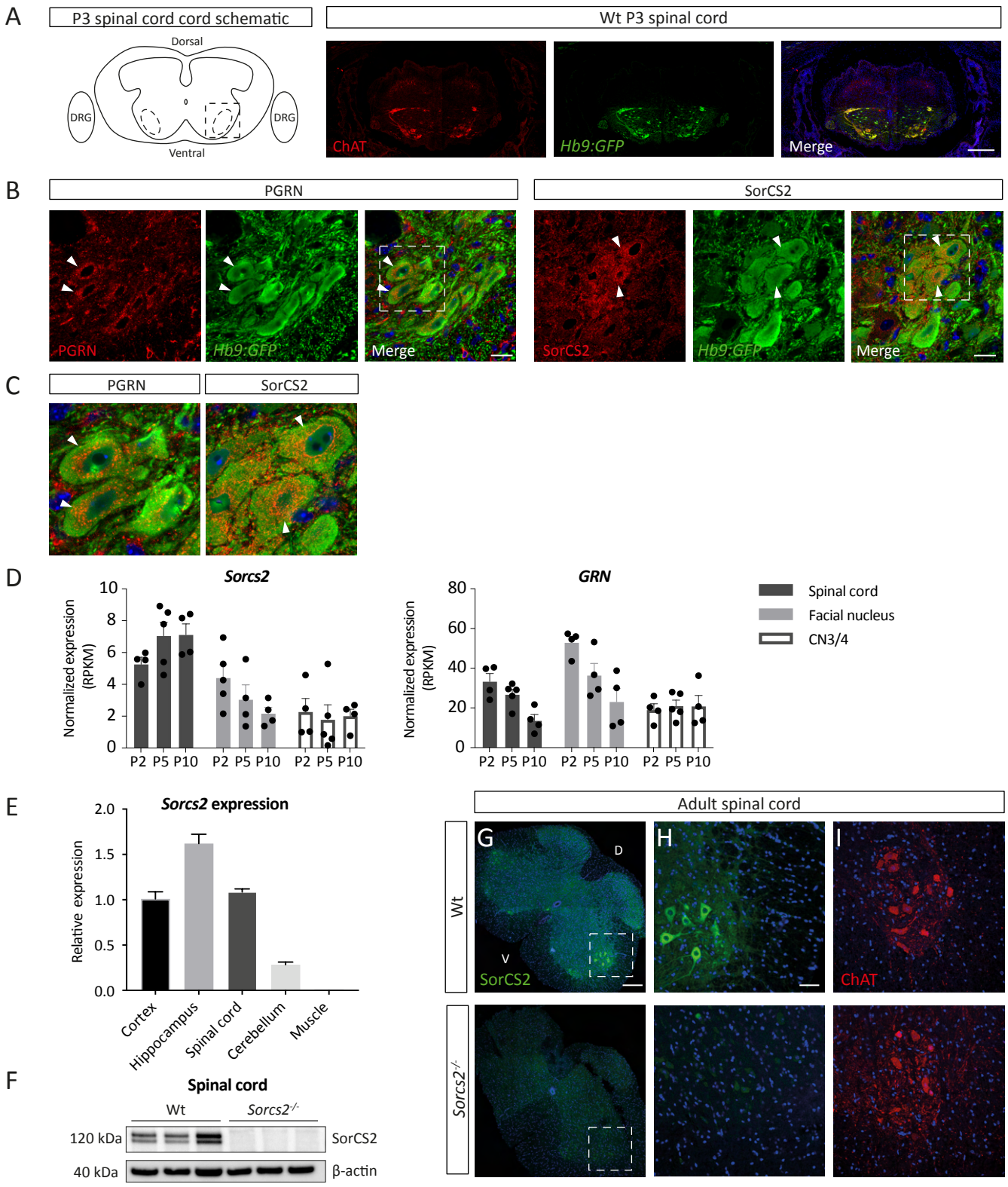
A
P3 spinal cord cord schematic
Dorsal
DRG
DRG
Ventral
Wt P3 spinal cord
ChAT
Hb9:GFP
Merge
B
PGRN
SorCS2
PGRN
Hb9:GFP
Merge
SorCS2
Hb9:GFP
Merge
C
PGRN
SorCS2
D
Sorcs2
Normalized expression (RPKM)
P2 P5 P10 P2 P5 P10 P2 P5 P10
GRN
Normalized expression (RPKM)
P2 P5 P10 P2 P5 P10 P2 P5 P10
Spinal cord
Facial nucleus
CN3/4
E
Sorcs2 expression
Relative expression
Cortex
Hippocampus
Spinal cord
Cerebellum
Muscle
Adult spinal cord
Wt
G
D
V
SorCS2
H
I
ChAT
Sorcs2-/-
F
Spinal cord
Wt
Sorcs2-/-
120 kDa
SorCS2
40 kDa
β-actin

807 **Figure 6: SorCS2 and PGRN are expressed in motor neurons postnatally**

808 **(A-C)** Immunofluorescent staining of horizontal P3 spinal cord sections from *Hb9::GFP* mice. (A) Left, illustration of
809 the section used. Right, ChAT (red) expression in GFP-labeled motor neurons confirming that Hb9 is also present in
810 postmitotic motor neurons. Scalebar = 200 µm. **(B)** Expression of PGRN (left) and SorCS2 (right) in Hb9-positive motor
811 neurons (arrow heads). Scalebar = 20 µm. Dashed squares are enlarged in **(C)**. Nuclei labeled with Hoechst in all sections.
812 **(D)** Transcriptional profiling of laser-captured motor neurons from the spinal cord, the facial nucleus, and the cranial
813 nuclei 3 and 4 from confirms *Grn* and *Sorcs2* expression in P2, P5, and P10 mice[46]. **(E)** RT-qPCR for *Sorcs2* expression
814 in cortex, hippocampus, spinal cord, cerebellum and muscle in 12 weeks old wt mice (n = 3). Relative expression indicates
815 fold-change normalized to cortical expression ($2^{-\Delta\Delta Ct}$), shown as mean ± s.e.m. **(F)** Immunoblotting for SorCS2 in spinal
816 cord demonstrates SorCS2 protein in Wt but not in *Sorcs2*$^{-/-}$ mice. β-actin serves as loading control. **(G)**
817 Immunofluorescent staining of SorCS2 in adult murine wt and *Sorcs2*$^{-/-}$ spinal cord sections. Scalebar = 200 µm. **(H)**
818 Enlargement of lateral ventral horn (white square). Motor neurons in wt but not *Sorcs2*$^{-/-}$ mice demonstrate SorCS2
819 expression (green). Scalebar = 50 µm. **(I)** Equivalent sections of ventral spinal cord showing ChAT expression (red) in
820 motor neurons. Nuclei are stained using Hoechst.

821

Figure 7

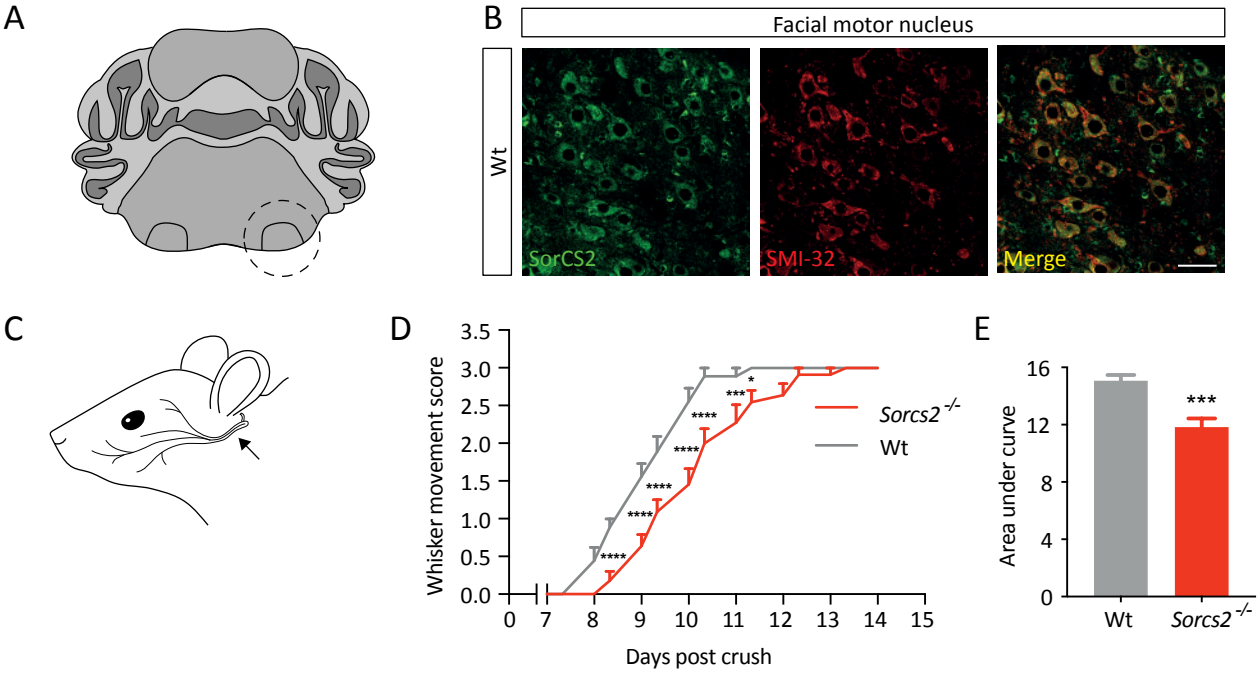

822 **Figure 7: *Sorcs2*$^{-/-}$ mice show delayed functional recovery after facial nerve crush injury**

823 **(A)** Illustration of the brain stem with the facial motor nuclei outlined. **(B)** Immunofluorescent staining of SorCS2 (green)
824 and the neuronal marker SMI-32 (red) in a section of the facial motor nucleus as outlined in panel (A) Scalebar = 50 µm.
825 (**C**) Schematic representation of the facial nerve and the injury site. (**D**) Regeneration of the facial nerve scored based on
826 whisker movement; 0: no movement, 1: detectable movement of individual whiskers, 2: significant but asymmetric
827 motion, 3: symmetric voluntary motion. Lack of SorCS2 significantly delays functional recovery after injury (two-way
828 ANOVA). (**E**) Area under the curve of whisker movement recovery scores is significantly reduced in *Sorcs2*$^{-/-}$ mice
829 (student's t-test) (n = 9,11). Data shown as mean ± s.e.m. **** < 0.0001, *** < 0.001, * < 0.05.

830

Figure 8

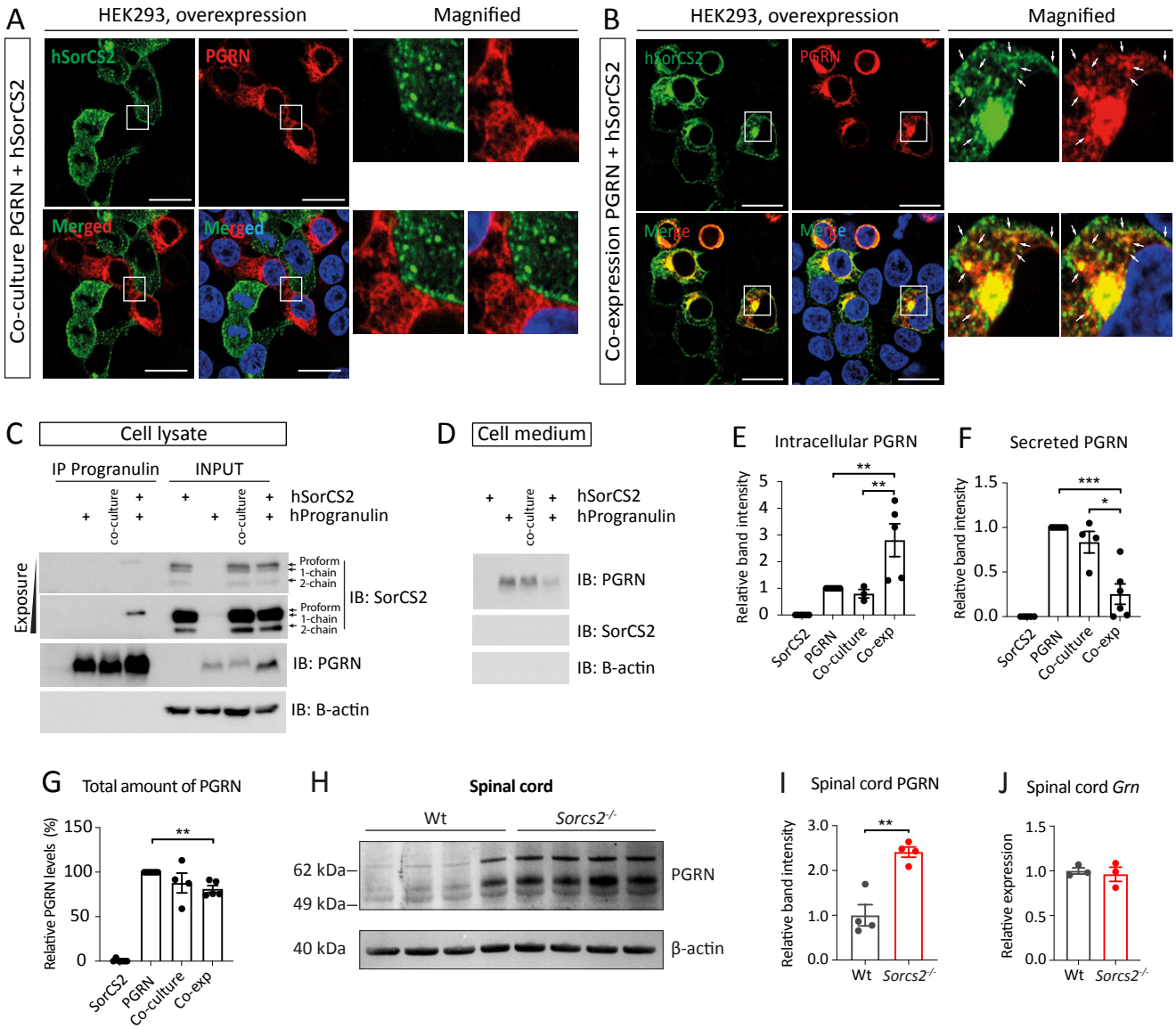

Figure 8: SorCS2 binds PGRN to control its secretion

(A-B) Immunofluorescence of HEK293 cells overexpressing human progranulin and SorCS2 separately and co-cultured (A) or co-expressing the receptors in the same cells (B). PGRN and SorCS2 do not colocalize on the plasma membrane when expressed separately (A), but they do so in Golgi-like compartments and vesicles when co-expressed in the same cells, highlighted by the arrows in (B). The nuclei are stained by Hoechst. Scalebar = 20 µm. **(C)** Co-immunoprecipitation of overexpressed SorCS2 and PGRN in HEK293 cells. SorCS2 physically binds PGRN intracellularly when co-expressed in the same cell (*cis*-configuration). The arrows point at three different isoforms of SorCS2 with the proform being accountable for the binding to PGRN. No co-IP is observed for the co-cultures **(D)** Representative immunoblots (IB) of the cell medium demonstrating secretion of PGRN. **(E-F)** In co-expressing cells, SorCS2 causes accumulation of PGRN intracellularly while reducing its secretion into the medium. The bars represent compiled quantification of the independent input samples blotted for PGRN (C+D) and HA in (S6C+D). The band intensity was measured as peak area (square pixel = 1) in ImageJ. **(G)** Total PGRN levels are decreased in cells co-expressing PGRN and SorCS2, quantified as combined relative band intensity from lysate and media (C+D). Immunoblots of β-actin serve as a loading control and negative control for the co-IP. P-value determined with Kruskal-Wallis test with uncorrected Dunn's multiple comparison test **(E-G)**. **(H)** Immunoblotting for PGRN shows increased levels in spinal cord from P3 *Sorcs2*$^{-/-}$ mice. **(I)** Quantification of immunoblots using loading control for normalization. P-value < 0.01 (student's t-test). **(J)** RT-qPCR of *Grn* expression in P3 spinal cord (n = 3). Relative expression indicates fold-change normalized to Wt ($2^{-\Delta\Delta Ct}$). Data shown as mean ± s.e.m. *** < 0.001, ** < 0.01, * < 0.05.

Figure S1

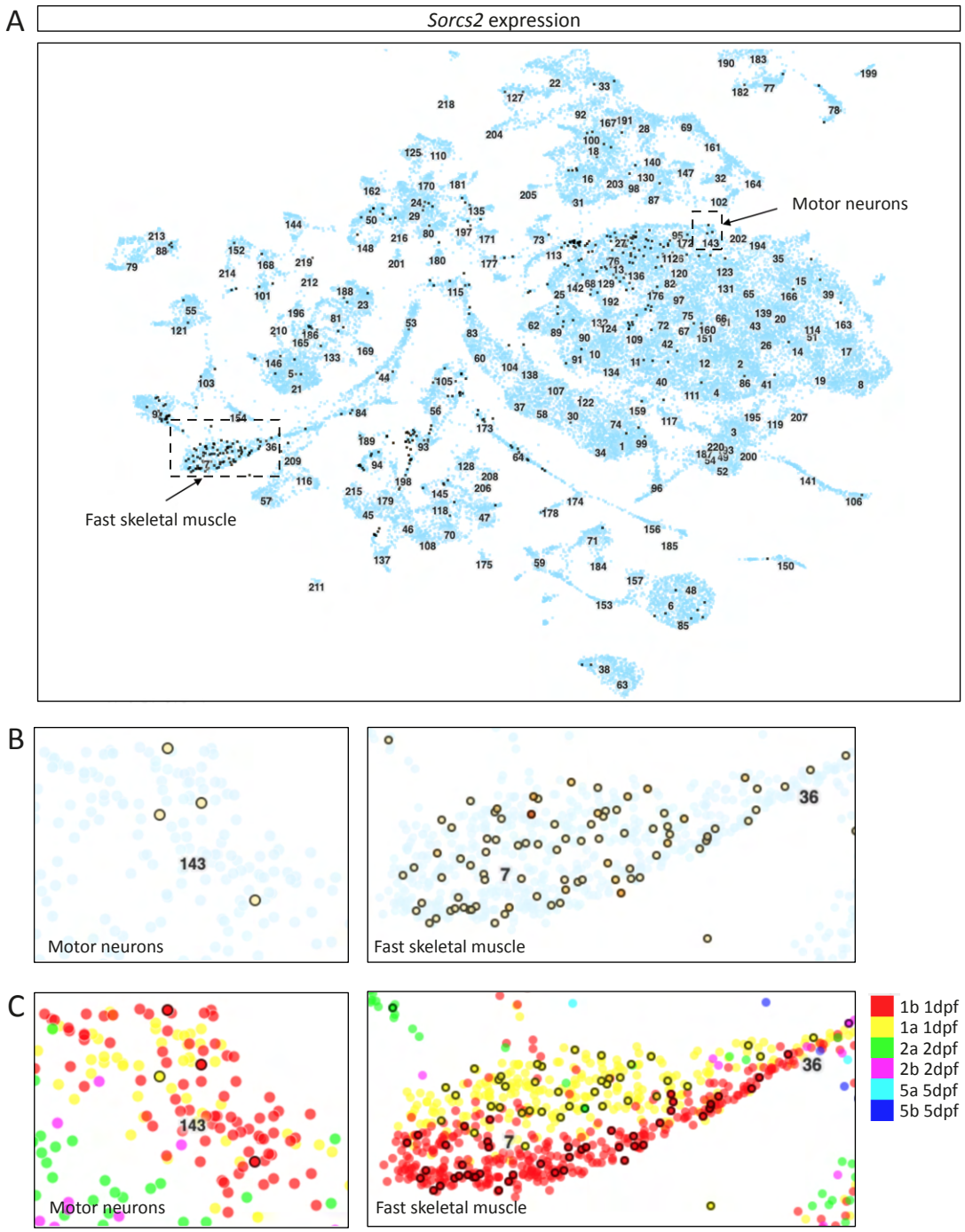

Figure S1: Single-cell transcriptome data of zebrafish *sorcs2*

Data from the single-cell transcriptome atlas of zebrafish embryos encompassing transcriptional profiles of 44,102 cells clustered according to cell type across four days of development[35]. **(A-C)** *Sorcs2* is expressed in different cell types including motor neurons and fast skeletal muscle in clusters 143, 7, and 36 (arrows). **(B)** Enlargement of dashed squares and with the age profile shown in **(C)**. dpf = days post fertilization.

Figure S2

855 **Figure S2:** Bright field images of a control MO and a *sorcs2* MO embryo at 25 hpf.

Figure S3

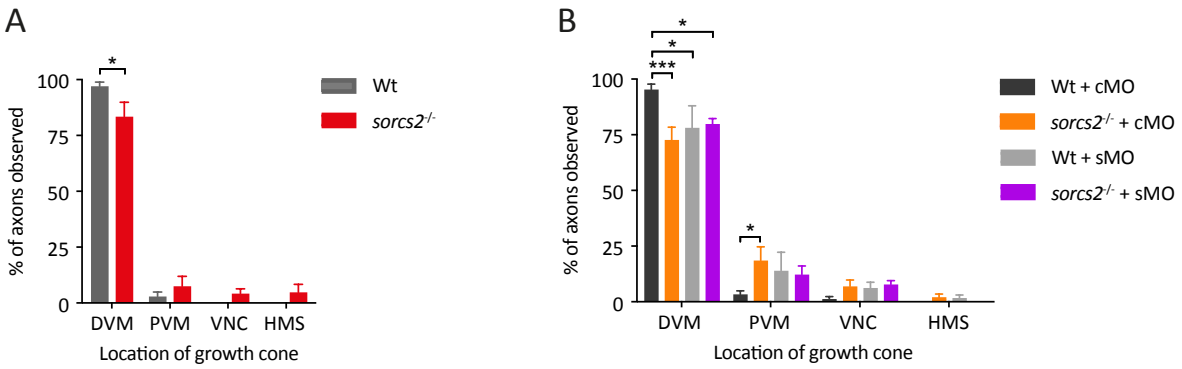

Figure S3: CaP axon outgrowth in *sorcs2*$^{-/-}$ zebrafish embryos

(A-B) Axon outgrowth in CaP axons from wt and *sorcs2*$^{-/-}$ embryos from heterozygous cross of *sorcs2*^{sa11642} zebrafish are shown in percentage. **(A)** *sorcs2*$^{-/-}$ axons (n = 6) are stunted compared to wt (n = 6) (p = 0.022). **(B)** Compared to wt + cMO (n = 6), axons from wt + sMO (n = 4, p = 0.011), *sorcs2*$^{-/-}$ + cMO (n = 4, p = 0.0005), and *sorcs2*$^{-/-}$ + sMO (n = 3, p = 0.047) are stunted. Injection of sMO into *sorcs2*$^{-/-}$ embryos does not aggravate the phenotype (73% vs. 80%, p = 0.670). Error bars: s.e.m., n = number of embryos. P-value determined with two-way ANOVA and Tukey's multiple comparisons. *** < 0.001, * < 0.05. HMS, horizontal myoseptum; VNC, ventral edge of notochord; PVM and DVM, distal and proximal ventral myotome.

Figure S4

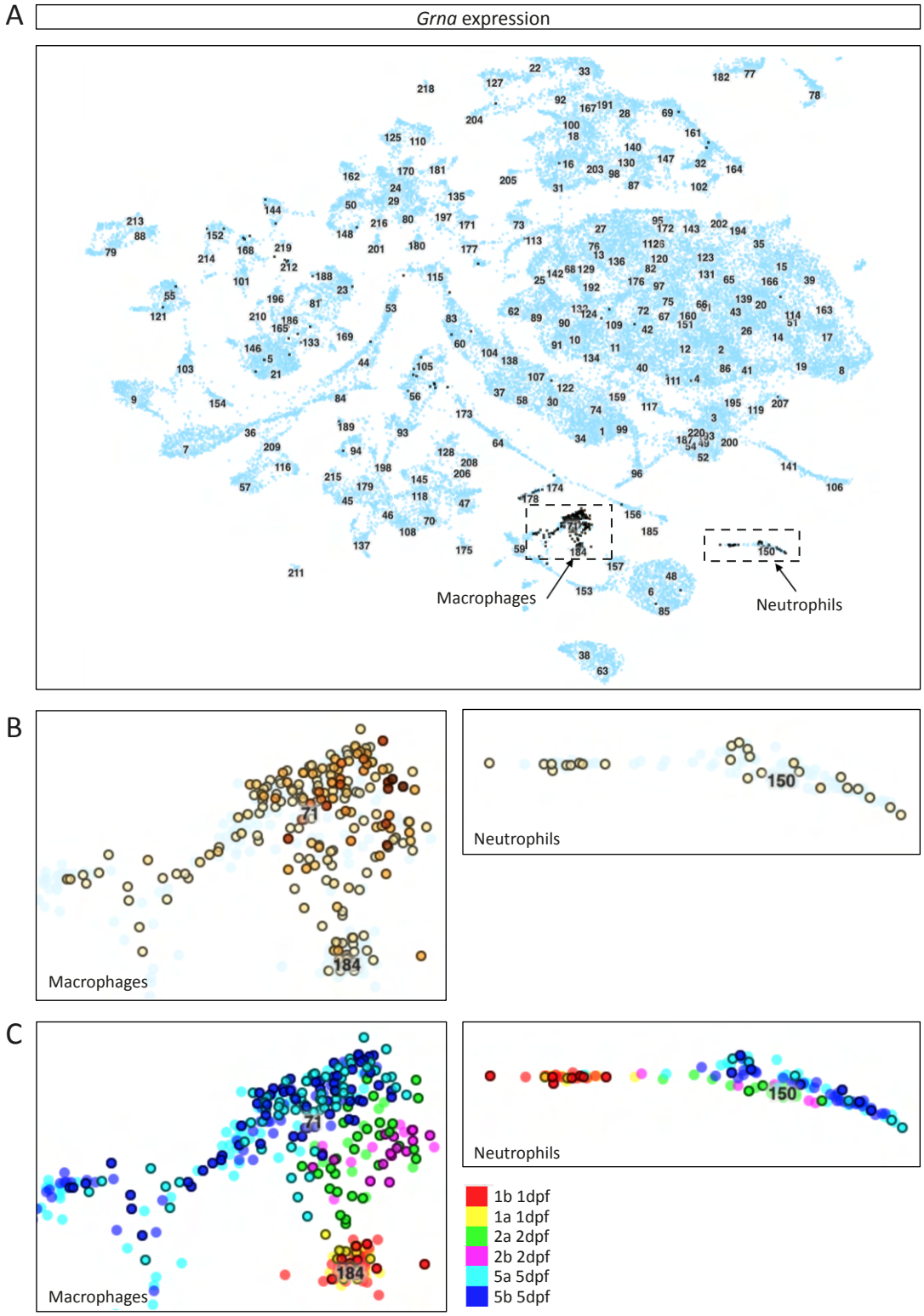

Figure S4: Single-cell transcriptome data of zebrafish *grna*

Data from the single-cell transcriptome atlas of zebrafish embryos encompassing transcriptional profiles of 44,102 cells clustered according to cell type across four days of development[35]. **(A-C)** *Grna* is mainly expressed in macrophages and neutrophils in clusters 71, 184, and 150 (arrows). **(B)** Enlargement of dashed squares and with the age profile shown in **(C)**. dpf = days post fertilization.

Figure S5

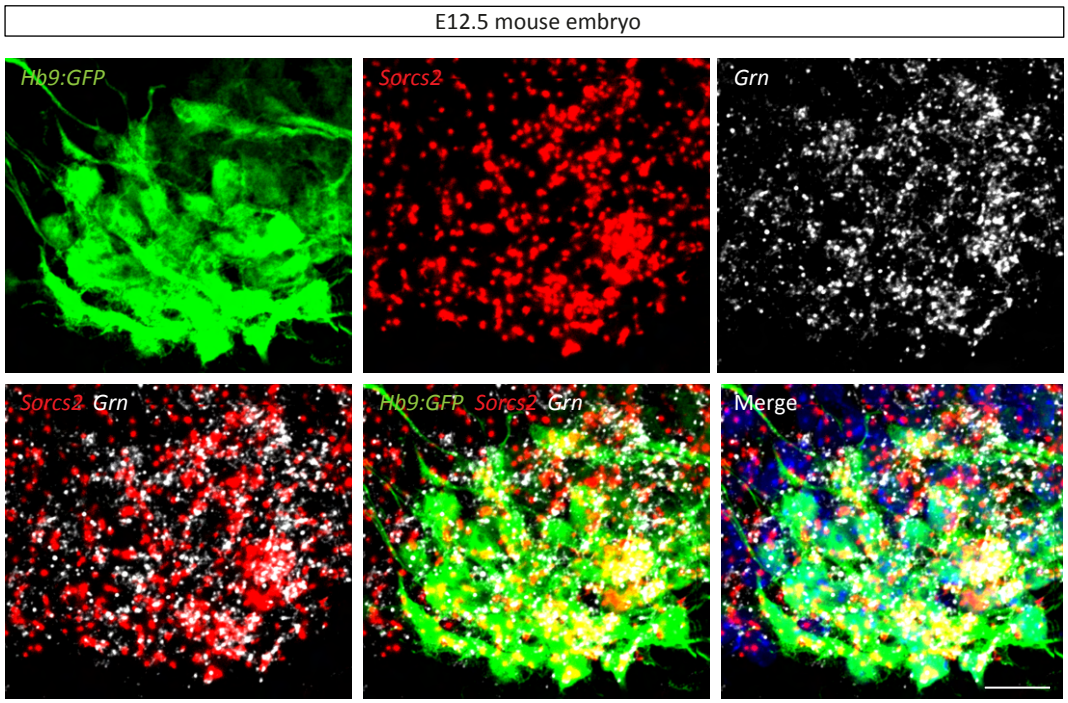

869 **Figure S5: RNA scope *in situ* hybridization of *Sorcs2* and *Grn***

870 RNA scope *in situ* hybridization of *Sorcs2* (red) and *Grn* (white) in horizontal sections of E12.5 *Hb9::GFP* mice.

871 Scalebar = 10 μm.

Figure S6

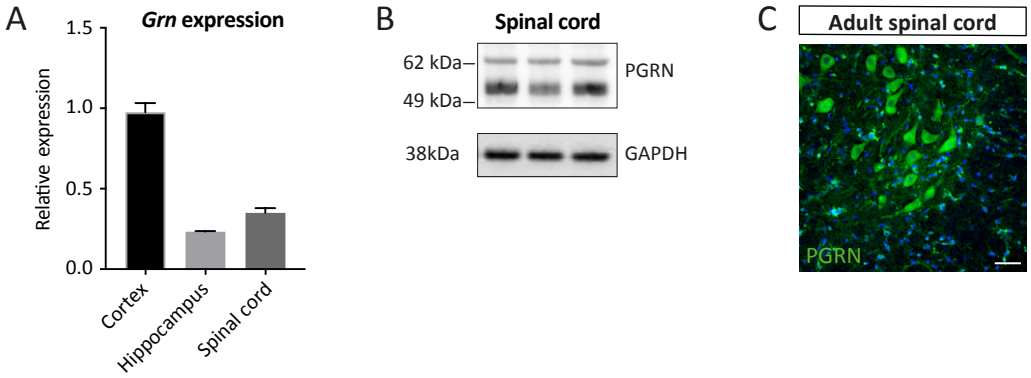

Figure S6: PGRN expression in adult murine spinal cord

(A) RT-qPCR for *Grn* expression in cortex, hippocampus, and spinal cord in 12 weeks old wt mice (n = 3). Relative expression indicates fold-change normalized to cortical expression ($2^{-\Delta\Delta Ct}$), shown as mean ± s.e.m. **(F)** Immunoblotting for PGRN in spinal cord demonstrates PGRN protein in Wt mice. GAPDH serves as loading control. **(G)** Immunofluorescent staining of PGRN in the lateral ventral spinal cord from an adult mouse showing PGRN (green) in motor neurons. Scalebar = 50 µm. Nuclei are stained using Hoechst.

Figure S7

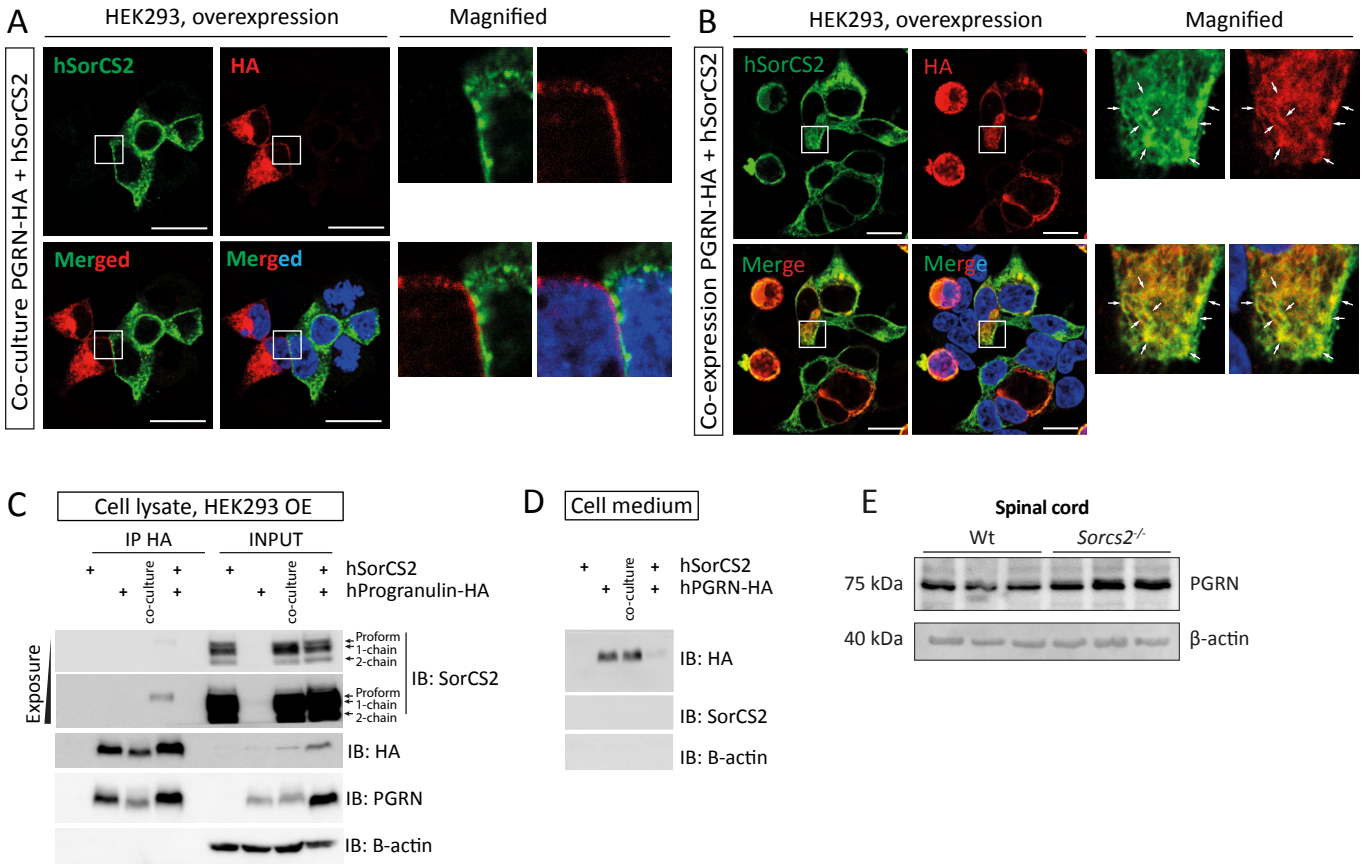

Figure S7: SorC2 and HA-PGRN binding and secretion

(A-B) Immunofluorescence of HEK293 cells overexpressing human HA-tagged PGRN (N-terminal tag) and SorCS2 separately and co-cultured (A) or co-expressing the receptors in the same cells (B). When expressed in *trans* (separately) there is no staining for PGRN at the plasma membrane in the SorCS2 expressing cells. (B) In *cis* (co-expression), SorCS2 co-localizes with HA-PGRN in Golgi-like compartments and vesicles as highlighted by the arrows in (B). The nuclei are stained using Hoechst. Scalebar = 20 µm. **(C)** Co-immunoprecipitation of SorCS2 with human HA-PGRN when co-expressed but not when expressed separately. The arrows point at three different isoforms of SorCS2 showing that the proform accounts for the binding to PGRN. **(D)** Immunoblots (IB) of the cell medium demonstrates secretion of PGRN. **(E)** Immunoblotting for PGRN shows that the levels in spinal cord from P3 *Sorcs2*$^{-/-}$ mice are increased. β-actin is used as loading control.

890 ## Supplementary movies

891 **Supplementary movie 1:** Live-imaging of a *sorcs2* KD *Tg(mnx1:GFP)*^{ml2} embryo from 18 to 38
892 hpf showing premature branching and truncation defects. Embryo oriented anterior to the right,
893 dorsal to the top.
894
895 **Supplementary movie 2:** Live-imaging of a control-injected *Tg(mnx1:GFP)*^{ml2} embryo from 20 to
896 38 hpf showing premature branching and truncation defects. Embryo oriented anterior to the right,
897 dorsal to the top.
898
899 **Supplementary movie 3:** Touch response of a 48 hpf control embryo after light touch in reduced
900 speed. Embryo uses 100 ms to swim 1 cm.
901
902 **Supplementary movie 4:** Touch response of a 48 hpf *sorcs2* KD embryo after light touch in
903 reduced speed. Embryo uses 170 ms to swim 1 cm.
904

905 # References

906 1. Stifani, N. Motor neurons and the generation of spinal motor neuron diversity. *Front. Cell. Neurosci.*
907 **8**, 1–22 (2014).
908 2. Bonanomi, D. Axon pathfinding for locomotion. *Semin. Cell Dev. Biol.* **85**, 26–35 (2019).
909 3. Gaudet, A. D., Popovich, P. G. & Ramer, M. S. Wallerian degeneration: Gaining perspective on
910 inflammatory events after peripheral nerve injury. *J. Neuroinflammation* **8**, 1–13 (2011).
911 4. Willnow, T. E., Petersen, C. M. & Nykjaer, A. VPS10P-domain receptors - regulators of neuronal
912 viability and function. *Nat. Rev. Neurosci.* **9**, 899–909 (2008).
913 5. Malik, A. R. & Willnow, T. E. VPS10P Domain Receptors: Sorting Out Brain Health and Disease.
914 *Trends Neurosci.* **43**, 870–885 (2020).
915 6. Rezgaoui, M. *et al.* Identification of SorCS2, a novel member of the VPS10 domain containing
916 receptor family, prominently expressed in the developing mouse brain. *Mech. Dev.* **100**, 335–8
917 (2001).
918 7. Hermey, G., Schaller, H. C. & Hermans-Borgmeyer, I. Transient expression of SorCS in developing
919 telencephalic and mesencephalic structures of the mouse. *Neuroreport* **12**, 29–32 (2001).
920 8. Hermey, G. *et al.* The three sorCS genes are differentially expressed and regulated by synaptic
921 activity. *J. Neurochem.* **88**, 1470–1476 (2004).
922 9. Oetjen, S., Mahlke, C., Hermans-Borgmeyer, I. & Hermey, G. Spatiotemporal expression analysis of
923 the growth factor receptor SorCS3. *J. Comp. Neurol.* **3402**, 3386–3402 (2014).
924 10. Boggild, S., Molgaard, S., Glerup, S. & Nyengaard, J. R. Highly segregated localization of the
925 functionally related vps10p receptors sortilin and SorCS2 during neurodevelopment. *J. Comp.*
926 *Neurol.* **526**, 1267–1286 (2018).
927 11. Boggild, S., Molgaard, S., Glerup, S. & Nyengaard, J. R. Spatiotemporal patterns of sortilin and
928 SorCS2 localization during organ development. *BMC Cell Biol.* **17**, 8 (2016).
929 12. Nykjaer, A. *et al.* Sortilin is essential for proNGF-induced neuronal cell death. *Nature* **427**, 843–8
930 (2004).
931 13. Glerup, S. *et al.* SorCS2 regulates dopaminergic wiring and is processed into an apoptotic two-chain
932 receptor in peripheral glia. *Neuron* **82**, 1074–87 (2014).
933 14. Deinhardt, K. *et al.* Neuronal growth cone retraction relies on proneurotrophin receptor signaling
934 through Rac. *Sci. Signal.* **4**, ra82 (2011).
935 15. Anastasia, A. *et al.* Val66Met polymorphism of BDNF alters prodomain structure to induce neuronal
936 growth cone retraction. *Nat. Commun.* **4**, 1–12 (2013).
937 16. Glerup, S. *et al.* SorCS2 is required for BDNF-dependent plasticity in the hippocampus. *Mol.*
938 *Psychiatry* **21**, 1740–1751 (2016).
939 17. Yang, J. *et al.* SorCS2 is required for social memory and trafficking of the NMDA receptor. *Mol.*

940 *Psychiatry* (2020). doi:10.1038/s41380-020-0650-7
941 18. Ma, Q. *et al.* SorCS2-mediated NR2A trafficking regulates motor deficits in Huntington's disease.
942 *JCI Insight* **2**, 1–16 (2017).
943 19. Kao, A. W., Mckay, A., Singh, P. P., Brunet, A. & Huang, E. J. Progranulin, lysosomal regulation
944 and neurodegenerative disease. *Nat. Publ. Gr.* **18**, 325–333 (2017).
945 20. Van Damme, P. *et al.* Progranulin functions as a neurotrophic factor to regulate neurite outgrowth
946 and enhance neuronal survival. *J. Cell Biol.* **181**, 37–41 (2008).
947 21. Ryan, C. L. *et al.* Progranulin is expressed within motor neurons and promotes neuronal cell survival.
948 *BMC Neurosci.* **10**, 130 (2009).
949 22. Martens, L. H. *et al.* Progranulin deficiency promotes neuroinflammation and neuron loss following
950 toxin-induced injury. *J. Clin. Invest.* **122**, 3955–3959 (2012).
951 23. Chitramuthu, B. P., Baranowski, D. C., Kay, D. G., Bateman, A. & Bennett, H. P. J. Progranulin
952 modulates zebrafish motoneuron development in vivo and rescues truncation defects associated with
953 knockdown of Survival motor neuron 1. *Mol. Neurodegener.* **5**, 41 (2010).
954 24. Laird, A. S. *et al.* Progranulin is neurotrophic in vivo and protects against a mutant TDP-43 induced
955 axonopathy. *PLoS One* **5**, e13368 (2010).
956 25. Chitramuthu, B. P., Kay, D. G., Bateman, A. & Bennett, H. P. J. Neurotrophic effects of progranulin
957 in vivo in reversing motor neuron defects caused by over or under expression of TDP-43 or FUS.
958 *PLoS One* **12**, e0174784 (2017).
959 26. Zhu, J. *et al.* CRISPR/Cas9-mediated grna gene knockout leads to neurodevelopmental defects and
960 motor behavior changes in zebrafish. *J. Neurochem.* **157**, 520–531 (2021).
961 27. Beel, S. *et al.* Progranulin functions as a cathepsin D chaperone to stimulate axonal outgrowth in
962 vivo. *Hum. Mol. Genet.* **26**, 2850–2863 (2017).
963 28. Baker, M. *et al.* Mutations in progranulin cause tau-negative frontotemporal dementia linked to
964 chromosome 17. *Nature* **442**, 916–919 (2006).
965 29. Cruts, M. *et al.* Null mutations in progranulin cause ubiquitin-positive frontotemporal dementia
966 linked to chromosome 17q21. *Nature* **442**, 920–924 (2006).
967 30. Zhou, X. *et al.* Impaired prosaposin lysosomal trafficking in frontotemporal lobar degeneration due to
968 progranulin mutations. *Nat. Commun.* **8**, 1–14 (2017).
969 31. Hu, F. *et al.* Sortilin-mediated endocytosis determines levels of the frontotemporal dementia protein,
970 progranulin. *Neuron* **68**, 654–667 (2010).
971 32. Zhou, X. *et al.* Prosaposin facilitates sortilin-independent lysosomal trafficking of progranulin. *J. Cell*
972 *Biol.* **210**, 991–1002 (2015).
973 33. Paushter, D. H., Du, H., Feng, T. & Hu, F. The lysosomal function of progranulin, a guardian against
974 neurodegeneration. *Acta Neuropathol.* **136**, 1–17 (2018).

975 34. Choi, H. M. T. *et al.* Third-generation in situ hybridization chain reaction: Multiplexed, quantitative,
976 sensitive, versatile, robust. *Dev.* **145**, (2018).
977 35. Farnsworth, D. R., Saunders, L. M. & Miller, A. C. A single-cell transcriptome atlas for zebrafish
978 development. *Dev. Biol.* **459**, 100–108 (2020).
979 36. Beattie, C. E. Control of motor axon guidance in the zebrafish embryo. **53**, 489–500 (2001).
980 37. Panzer, J. A. *et al.* Neuromuscular synaptogenesis in wild-type and mutant zebrafish. **285**, 340–357
981 (2005).
982 38. Goody, M. F. *et al.* NAD+ Biosynthesis Ameliorates a Zebrafish Model of Muscular Dystrophy.
983 *PLoS Biol.* **10**, (2012).
984 39. Arber, S., Han, B., Mendelsohn, M., Smith, M. & Jessell, T. M. Requirement for the Homeobox Gene
985 Hb9 in the Consolidation of Motor Neuron Identity spinal MNs exhibit several levels of organization
986 and function (Landmesser, 1978a, 1978b), and these have a molecular correlate in the selective
987 patterns of expres. *Neuron* **23**, 659–674 (1999).
988 40. Li, L., Xiong, W.-C. & Mei, L. Neuromuscular Junction Formation, Aging, and Disorders. *Annu. Rev.*
989 *Physiol.* **80**, 159–188 (2018).
990 41. Rousso, D. L., Gaber, Z. B., Wellik, D., Morrisey, E. E. & Novitch, B. G. Coordinated Actions of the
991 Forkhead Protein Foxp1 and Hox Proteins in the Columnar Organization of Spinal Motor Neurons.
992 *Neuron* **59**, 226–240 (2008).
993 42. Wiese, S. *et al.* Isolation and enrichment of embryonic mouse motoneurons from the lumbar spinal
994 cord of individual mouse embryos. *Nat. Protoc.* **5**, 31–38 (2009).
995 43. Gass, J. *et al.* Progranulin regulates neuronal outgrowth independent of Sortilin. *Mol. Neurodegener.*
996 **7**, 1–13 (2012).
997 44. Inglis, F. M., Zuckerman, K. E. & Kalb, R. G. Experience-dependent development of spinal motor
998 neurons. *Neuron* **26**, 299–305 (2000).
999 45. Feng, T. *et al.* Loss of TMEM 106B and PGRN leads to severe lysosomal abnormalities and
1000 neurodegeneration in mice . *EMBO Rep.* **21**, 1–24 (2020).
1001 46. Nichterwitz, S. *et al.* LCM-seq reveals unique transcriptional adaptation mechanisms of resistant
1002 neurons and identifies protective pathways in spinal muscular atrophy. *Genome Res.* **30**, 1083–1096
1003 (2020).
1004 47. Malik, A. R. *et al.* SorCS2 Controls Functional Expression of Amino Acid Transporter EAAT3 and
1005 Protects Neurons from Oxidative Stress and Epilepsy-Induced Pathology. *Cell Rep.* **26**, 2792-2804.e6
1006 (2019).
1007 48. Tang, W. *et al.* The growth factor progranulin binds to TNF receptors and is therapeutic against
1008 inflammatory arthritis in mice. *Science* **332**, 478–84 (2011).
1009 49. Park, B. *et al.* Granulin Is a Soluble Cofactor for Toll-like Receptor 9 Signaling. *Immunity* **34**, 505–

1010 513 (2011).
1011 50. Neill, T. *et al.* EphA2 is a functional receptor for the growth factor progranulin. *J. Cell Biol.* **215**,
1012 687–703 (2016).
1013 51. Altmann, C. *et al.* Progranulin promotes peripheral nerve regeneration and reinnervation: Role of
1014 notch signaling. *Mol. Neurodegener.* **11**, 1–22 (2016).
1015 52. De Muynck, L. *et al.* The neurotrophic properties of progranulin depend on the granulin E domain but
1016 do not require sortilin binding. *Neurobiol. Aging* **34**, 2541–2547 (2013).
1017 53. Campbell, C. A. *et al.* A zebrafish model of granulin deficiency reveals essential roles in myeloid cell
1018 differentiation. *Blood Adv.* **5**, 796–811 (2021).
1019 54. Petkau, T. L. *et al.* Progranulin expression in the developing and adult murine brain. *J. Comp. Neurol.*
1020 **518**, 3931–3947 (2010).
1021 55. Hyung, S. *et al.* Dedifferentiated Schwann cells secrete progranulin that enhances the survival and
1022 axon growth of motor neurons. *Glia* **67**, 360–375 (2019).
1023 56. Banerjee, S. *et al.* A novel role for MuSK and non-canonical wnt signaling during segmental neural
1024 crest cell migration. *Development* **138**, 3287–3296 (2011).
1025 57. Nagy, N. *et al.* Collagen 18 and agrin are secreted by neural crest cells to remodel their
1026 microenvironment and regulate their migration during enteric nervous system development. *Dev.* **145**,
1027 (2018).
1028 58. Zhu, J. *et al.* Conversion of Proepithelin to Epithelins. *Cell* **111**, 867–878 (2002).
1029 59. Nykjaer, A. & Willnow, T. E. Sortilin: a receptor to regulate neuronal viability and function. *Trends*
1030 *Neurosci.* **35**, 261–70 (2012).
1031 60. Teng, H. K. ProBDNF Induces Neuronal Apoptosis via Activation of a Receptor Complex of
1032 p75NTR and Sortilin. *J. Neurosci.* **25**, 5455–5463 (2005).
1033 61. Evans, S. F. *et al.* Neuronal brain-derived neurotrophic factor is synthesized in excess, with levels
1034 regulated by sortilin-mediated trafficking and lysosomal degradation. *J. Biol. Chem.* **286**, 29556–67
1035 (2011).
1036 62. Chen, Z. Y. *et al.* Sortilin controls intracellular sorting of brain-derived neurotrophic factor to the
1037 regulated secretory pathway. *J. Neurosci.* **25**, 6156–6166 (2005).
1038 63. Kettleborough, R. N. W. *et al.* A systematic genome-wide analysis of zebrafish protein-coding gene
1039 function. *Nature* **496**, 494–7 (2013).
1040 64. Breacker, C., Barber, I., Norton, W. H. J., Mcdearmid, J. R. & Tilley, C. A. A Low-Cost Method of
1041 Skin Swabbing for the Collection of DNA Samples from Small Laboratory Fish. **14**, 1–8 (2017).
1042 65. Kimmel, C. B., Ballard, W. W., Kimmel, S. R., Ullmann, B. & Schilling, T. F. Stages of embryonic
1043 development of the zebrafish. *Dev. Dyn.* **203**, 253–310 (1995).
1044 66. Robu, M. E. *et al.* p53 Activation by Knockdown Technologies. **3**, (2007).

1045 67. Thisse, C. & Thisse, B. High-resolution in situ hybridization to whole-mount zebrafish embryos. **3**,
1046 59–69 (2008).
1047 68. Lauter, G., Söll, I. & Hauptmann, G. Two-color fluorescent in situ hybridization in the embryonic
1048 zebrafish brain using differential detection systems. *BMC Dev. Biol.* **11**, 43 (2011).
1049 69. Beck, A. P., Watt, R. M. & Bonner, J. Dissection and lateral mounting of zebrafish embryos: analysis
1050 of spinal cord development. *J. Vis. Exp.* e50703 (2014). doi:10.3791/50703
1051 70. Schindelin, J. *et al.* Fiji - an Open platform for biological image analysis. *Nat. Methods* **9**, (2009).
1052 71. Liu, C., Ma, W., Su, W. & Zhang, J. Prdm14 acts upstream of islet2 transcription to regulate axon
1053 growth of primary motoneurons in zebrafish. *Development* **139**, 4591–600 (2012).
1054 72. Hilario, J. D., Rodino-Klapac, L. R., Wang, C. & Beattie, C. E. Semaphorin 5A is a bifunctional axon
1055 guidance cue for axial motoneurons in vivo. *Dev. Biol.* **326**, 190–200 (2009).
1056 73. Jing, L. Flourescent Immunostaining Protocol for a-Bungorotoxin (AChRs) in Zebrafish. *BIO-*
1057 *PROTOCOL* **2**, 20–21 (2012).
1058 74. Catela, C., Shin, M. M., Lee, D. H., Liu, J. P. & Dasen, J. S. Hox Proteins Coordinate Motor Neuron
1059 Differentiation and Connectivity Programs through Ret/Gfrα Genes. *Cell Rep.* **14**, 1901–1915 (2016).
1060 75. Salašová, A. *et al.* A proteomic analysis of LRRK2 binding partners reveals interactions with
1061 multiple signaling components of the WNT/PCP pathway. *Mol. Neurodegener.* **12**, 1–19 (2017).
1062